Habilitationsschrift

zur

Erlangung der Venia legendi

für das Fach Physik

der

Ruprecht-Karls-Universität

Heidelberg

vorgelegt von

Dr. Sven Sturm

aus Koblenz

11.10.2021

Penning trap experiments for fundamental atomic physics

Abstract

The possibility to store charged particles in Penning traps for long times basically at rest has enabled a rich variety of intriguing measurement opportunities. The purely static magnetic and electric fields, in combination with the extremely good vacuum in cryogenic Penning traps, largely decouples the ion from the complicated environment and thus gives a clear and unobscured view onto the fundamental properties of the ion. Moreover, the theoretical calculations in atomic physics, using the quantum field theories of the Standard Model, have reached an impressive precision. Consequently, by measuring observables with similar precision we get the opportunity to test our most fundamental theories in physics. Here, highly charged ions (HCI) play a special role. The bound electrons in such HCI are exposed to the extremely strong electromagnetic fields of the nucleus - the strongest fields we have available in the laboratory in stable systems. Moreover, in HCI typically only single or a few electrons are left and calculations of the atomic structure are relatively simple and accurate. Consequently, HCI provide close to ideal conditions for stringent tests of the Standard Model, specifically quantum electrodynamics (QED). In the last years, my group at the Max Planck Institute for Nuclear Physics (MPIK), part of the "stored and cooled ions" division led by Klaus Blaum, has developed two experiments, ALPHATRAP and LIONTRAP. LIONTRAP is dedicated to the determination of the atomic masses of the lightest ions. We have provided world-leading values for the proton, the deuteron and the HD^+ molecular ion. This way, we have shed light on the puzzle of light ion masses, a long-standing discrepancy in the literature values of these fundamentally important constants. At ALPHATRAP and its predecessor experiment at Mainz we have performed a series of measurements on the g-factor of the bound electron(s), among others the to date most stringent test of QED in strong fields and the determination of the electron atomic mass from the g-factor of hydrogenlike carbon to 11 digits. Recently, we have connected ALPHATRAP to the Heidelberg HD-EBIT high energy ion source and are now working on progressing our experiments towards the heavy-HCI regime, where electric fields up to $10^{16}\ \mathrm{V\,cm^{-1}}$ can be found. With this programme, ALPHATRAP is part of the Collaborative Research Centre 1225 ISOQUANT. Furthermore, new techniques enable performing precise laser spectroscopy in HCI and other systems that are notoriously difficult to address, such as the molecular hydrogen ion. The development of sympathetic laser cooling of ions in separate traps will open up a precision regime that was previously beyond reach. Overall, we have a unique toolbox available, which will give us the opportunity to perform intriguing measurements that will help to advance our understanding of fundamental physics.

Contents

Glossary

g-factor unitless gyromagnetic ratio, $\vec{\mu} = \frac{q}{2m}\vec{s}$.

BWE Bohr-Weisskopf effect, the influence of the spatial distribution of the nuclear magnetization on the hyperfine splitting.

CFR cyclotron frequency ratio.

CPT charge parity time.

CSGE continuous Stern-Gerlach effect, allows determination of the spin orientation via a superimposed magnetic bottle.

ESR Experimental storage ring.

FWHM Full width at half maximum.

HCI highly charged ion.

HFS Hyperfine splitting or hyperfine structure.

KATRIN Karlsruhe Tritium Neutrino Experiment, Experiment to determine the electron-antineutrino mass from the beta decay spectrum of tritium.

mmW millimeter waves, microwaves with a wavelength in the single mm range.

MPIK Max-Planck-Institut für Kernphysik (Max Planck Institute for Nuclear Physics).

OFHC Oxygen-Free High thermal Conductivity, a copper alloy with < 500 ppm of oxygen content.

PnA Pulse-and-Amplify, phase sensitive frequency estimation technique specifically for low energies.

PnP Pulse-and-Phase, phase sensitive frequency estimation technique.

ppm parts per million, 10^{-6}.

QED quantum electrodynamics, the quantum field theory to describe the electromagnetic interaction within the standard model.

QLS quantum logic spectroscopy.

SODS second order Doppler shift.

SQUID superconducting interference device.

w.l.o.g. without loss of generality.

XHV eXtremely High Vacuum.

1 | Introduction

Over the last decades, Penning traps have evolved into a very versatile and powerful tool to perform ultra precision measurements on charged particles [1]. The simplicity of the static electromagnetic fields which provide the confinement enables an unparalleled control of the motional frequencies of the trapped particles. Especially in cryogenic setups, where cryosorption of the residual gas enables achieving a virtually perfect vacuum below 10^{-16} mbar, we can engineer traps with properties almost indistinguishable from the ideal mathematical concept. The trapped particle can be isolated from the environment to an extent where only desired interactions play a role. This is obviously very close to the ideal spectroscopic situation that Hans G. Dehmelt depicted of a single, isolated particle, resting in empty space [2]. Making use of this toolbox allows us to measure observables of atomic physics with exceptional precision. By comparing those observables with predictions of quantum theory we can put our understanding of physics to a delicate test. Since only dimensionless quantities can be of truely fundamental meaning it is typically ratios of observables, in many cases measured with different systems and in independent experiments, that have to be combined in order to perform such a test. This way, automatically a large range of physics is tested.

The large magnitude of the confining magnetic field B in Penning traps, typically in the range of several tesla, naturally provides access to properties of the ion that are related to the magnetic field strength. The cyclotron frequency $\omega_c = \frac{q}{m}B$ with which the ion (with charge q and mass m) would rotate around the axis of the homogeneous magnetic field plays a key role in that context, as it enables calibrating the magnetic field strength right at the position of the ion with high precision. This way, a number of intriguing measurements become possible, such as determinations of the charge-to-mass ratio ("mass measurements") or, if the mass of the particle is known sufficiently well, the magnetic moment of the particles[1]. A seminal example of this concept is the determination of $a_e = (g-2)/2$ [3, 4], the anomaly of the electron spin. Here, the small difference between the frequencies of the cyclotron rotation and the precession of the electron spin is determined. As the spin precession (Larmor) frequency is proportional to the g-factor of the electron, which can be calculated from first principles and with extraordinary precision using quantum electrodynamics (QED), a comparison of the measured anomaly with

[1] If the magnetic moment is given in the form of the dimensionless g-factor, for "fundamental" particles such as the electron, but also e.g. the proton, the mass drops out in the definition and its precise knowledge is thus not required.

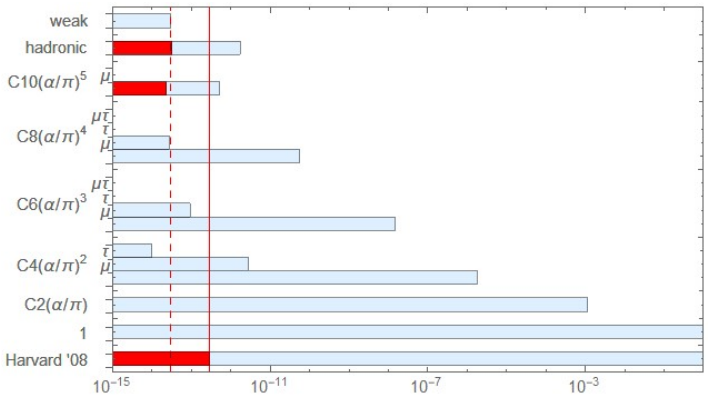

Figure 1.1: Contributions to $g/2$ of the electron. With higher precision, not only higher loop-order QED contributions, but also contributions originating from weak and strong interactions become visible. Taken from [10].

the theoretical prediction yields a sensitive and stringent test of the Standard Model. Already in 1987 Hans G. Dehmelt had developed the techniques necessary to confine a single electron indefinitely, observe its motional frequencies via their associated image currents and to determine its spin orientation via a technique termed the "continuous Stern-Gerlach effect" (CSGE [5], see section 2.4). With this toolbox, Dehmelt was able to measure the anomaly a_e of the electron in absence of disturbances from other charged particles and in a very clean and controlled environment. He achieved a relative accuracy of about 4 ppb[2] for both the electron and its antimatter counterpart, the positron [3]. When using a value of the electromagnetic finestructure constant α from an independent measurement with comparable precision, as it is available today [6, 7], this result can be interpreted as a test (and confirmation) of quantum electrodynamics on that level. In 2006 [8] and 2008 [4], the group of Gerald Gabrielse at Harvard further improved on this precision and achieved the to date most precise value for a_e with a relative uncertainty of only 0.28 ppb. Here, a general property of this class of experiments becomes apparent: As the observable, in this case the anomaly of the electron or positron, is (potentially) influenced by a large variety of effects from QED but also weak and strong interactions as well as hypothetical unknown particles and interaction ("fifth force" [9]) on some level, an improved experimental (and theoretical) precision can be seen as a more stringent probe for any physics beyond the Standard Model. Indeed, the precision in such low energy experiments (and generally atomic physics experiments) can be sufficient to compete with or exceed the stringency of searches for new physics with high energy experiments in large scale accelerators and impose important constraints on the development of theories beyond the Standard Model [11]. A similar measurement as for the electron anomaly can also be performed for the muon, the next-heavier lepton. Owing to the finite lifetime and the production mechanism of the muon, this measurement is performed in a storage ring [12] at Fermilab. While the muon g-2 is significantly less precise than the electron

[2]parts per billion

version, the most recent run of the experiment has produced a result at .46 ppm[3] relative precision. Combined with earlier results [13] from the same storage ring, operated at Brookhaven National Laboratory at that time, the precision reaches 0.35 ppm and reveals a tension with the theoretical prediction of about 4.2 standard deviations. This is especially intriguing as the muon is, compared to the electron, more sensitive to unknown particles by a factor of $(m_\mu/m_e)^2 \approx 43\,000$. The collaboration is currently working on the evaluation of data already taken in additional runs. Once revealed, these will either make the current discrepancy vanish or unambiguously confirm a hint on new physics. In that case, more experiments on other observables will be required to gain further insight into the nature of this discrepancy. A special type of experiment are comparisons of the same property in a matter and antimatter particle. Here, charge-parity-time (CPT) reversal symmetry demands that both values need to be identical (up to the sign). This way, a test of CPT invariance does not necessarily need a theoretical prediction of the value of the observable. In the case of the electron and positron the values of the anomalies have been compared and found to be equal at the given precision - which lead to the most stringent test of CPT invariance in the lepton sector [3]. Furthermore, the charge-to-mass ratio of proton and antiproton has been compared [14] in a Penning trap by the BASE collaboration at the antiproton decelerator at CERN, Geneva.

A wealth of very interesting observables arise when using composite atomic or molecular ions in Penning trap experiments. While e.g. in the case of the g-factor the observable spin precession frequency depends on an external parameter, in this case the magnetic field, in atomic and molecular ions the internal binding fields define observables. While a magnetic field, even from the best superconducting magnet, will always show fluctuations in time, the atomic fields are stable to a much higher extent, only limited by external perturbations. Consequently, also the transition frequencies can be measured with - in many cases - higher precision. A spectacular example are the optical ion clocks, which now have surpassed a fractional repeatability of $\delta f/f = 10^{-18}$ [15]. However, especially for heavy ions, the increasing number of electrons makes it very challenging to perform calculations with comparable precision. There is only a limited number of observables that can be assessed from first principles. Here, highly charged ions (HCI) play an important role. By removing most of the electrons from a heavy ion, not only the complexity of the system is drastically reduced, but the remaining electrons are then located in the inner shells - where they are exposed to the strongest electromagnetic fields accessible to precision experiments in the laboratory. The electric field in hydrogenlike $^{208}Pb^{81+}$ ion reaches 10^{16} V/cm, orders of magnitude higher than in the currently most intense lasers. This allows us to assess the question whether QED - which had originally been constructed (and tested) with only weak or even negligible fields available - stays valid even in the most extreme conditions.

[3] parts per million

Experimentally, such highly charged ions bring along new challenges. The transitions of the gross structure scale quadratically with the nuclear charge Z, bringing them into the regime of hard x-rays for heavy systems. Consequently, the high precision offered by optical spectroscopy techniques can be only applied to special types of transitions (see chapter 5). The spin precession frequency is however not subject to this strong scaling, so that the g-factor of the HCI remains an extremely useful observable for tests of physics in strong fields. Before performing spectroscopy however, the ions have to be produced, which becomes increasingly difficult with higher nuclear charge Z as the ionisation potential increases roughly proportional to Z^2 and surpasses hundred keV for hydrogenlike $^{208}Pb^{81+}$. Only very few facilities worldwide have the ability to produce such ions. At the GSI Helmholtzzentrum für Schwerionenforschung the (lowly charged) ions are accelerated to high energy and then impinged onto a thin foil, where they loose most of their electrons. While this is very efficient in producing HCI, the products have a large energy distribution and are consequently hard to capture. The HITRAP facility [16] is aiming at this task. The alternative is to keep the ions essentially at rest and impinge them with a high-energy electron beam. To achieve substantial production rates in this concept of an electron beam ion trap (EBIT), a very intense, high-energy electron beam is required. An EBIT that potentially meets this requirement is the Heidelberg HD-EBIT at the Max Planck Institute for Nuclear Physics (MPIK) in Heidelberg, Germany, developed and run by the group of Prof. Dr. José Crespo.

The unique conditions at MPIK also provided the foundations that allowed my group, a part of the "stored and cooled ions" division lead by Prof. Dr. Klaus Blaum, to develop and build Alphatrap [1], a cryogenic multi-Penning trap setup dedicated to precision measurements with HCI for fundamental physics. This versatile experiment is based on the original g-factor experiment for HCI that has been developed and built at the Johannes Gutenberg University Mainz by a collaboration between Prof. Dr. Günter Werth, PD. Dr. Wolfgang Quint and Prof. Dr. Heinz-Jürgen Kluge and later has been further developed by the group of Klaus Blaum, including myself during my PhD thesis. Unlike this original experiment however, Alphatrap allows the injection of ions from the HD-EBIT and other external sources and provides optical access to the trap, in addition to the millimeter-wave access. In a special "analysis trap" with a strong magnetic bottle we can employ the CSGE to determine the magnetic moment orientation of the ion. This way, a multitude of different measurements can be performed at Alphatrap, from g-factor measurements to optical spectroscopy. As we have recently proposed [1, 17], we can use the CSGE to find and probe even extremely long-lived and correspondingly narrow transitions. Owing to a cryogenically operable valve, Alphatrap reaches the extremely good vacuum level required for the long-term confinement of even the heaviest ions in spite of its connection to a room-temperature beamline for ion injection. This unique combination of features

has already lead to very successful measurements in the past years [18, 17] and will in the future allow us to perform extraordinarily stringent tests of QED in strong fields. To this end, the experimental results have to be complemented with the best theory predictions. To this end, my group is embedded in the project B01 of the Collaborative Research Centre 1225 ISOQUANT. Here, we strongly profit from the close collaboration with the theory group of PD. Dr. Zoltán Harman in the ISOQUANT project B02, one of the world-leading groups in this field. Furthermore, we have long-term collaborations with a number of theory groups worldwide that are working on this subject, among others Vladimir Shabaev and Dmitry Glazov in St. Petersburg, Andrey Volotka at the Helmholtz Insitute in Jena and Krzysztof Pachucki at the University of Warsaw.

While ALPHATRAP is optimised for heavy HCI, for many applications in atomic physics the masses of specifically the lightest ion - proton, deuteron and the helium isotopes are required. A value of the proton (and deuteron) mass, combined with an independently measured electron mass, enables the interpretation of the extremely precisely measured spectra of the hydrogen atom and the hydrogen molecular ions [19, 20, 21]. In this range of masses, the precision achieved today exceeds 10 ppt, which corresponds to about 10 meV of energy when expressed as the equivalent mass increase. This means that atomic scale energies can be weighed as masses. By comparing the ground state mass of $^3He^+$ and $^3T^+$ we plan to give a precise measure of the energy released by the beta decay of $^3T^+$. This value is of importance for the KATRIN collaboration as an independent calibration of the endpoint of this decay in the search for the electron anti-neutrino mass.

In order to enable measurements specifically in this light mass regime, a specialised apparatus is required. When the available electron beam energy in the hermetically sealed trap chamber of the Mainz g-factor experiment on HCI became a limitation for extending these measurements towards higher Z HCI, our group started an extensive reconstruction of this apparatus. The result is the LIONTRAP (Light Ion Trap) experiment, a cryogenic Penning trap system dedicated and optimized to mass measurements on light ions. This thesis will give an overview of measurements that have been performed by these two setups and how these have contributed to the current state of knowledge in atomic physics. Chapter 2 is dedicated to the basic principles of Penning trap measurements and introduces the techniques used here. In chapter 3, 4 and 5 LIONTRAP and ALPHATRAP and their most successful measurement campaigns are presented. Finally, in chapter 6 I give an outlook onto the exciting future of this field.

2 | Basics of Precision Penning-Trap Experiments

In this chapter I will give a brief introduction of the common techniques and the nomenclature commonly used in modern precision Penning-trap experiments. More information in a consistent notation can be found in our extensive review articles on the ALPHATRAP g-factor experiment

- S. Sturm et al. "The ALPHATRAP experiment". In: *Eur. Phys. J. Spec. Top.* 227.13 (2019), pp. 1425–1491

as well as the LIONTRAP mass spectrometer

- F. Heiße et al. "High-precision mass spectrometer for light ions". In: *Phys. Rev. A* 100 (2 2019), p. 022518

The latter article also covers the known dominant systematic frequency shifts of LIONTRAP.

In a Penning trap a charged particle with mass m and charge q is confined mainly by a strong homogeneous magnetic field B_0, typically of several tesla strength and generated by a superconducting magnet, which forces the particle onto cyclotron-like spiral orbits *around* the magnetic field axis (z axis) with a frequency[1]

$$\omega_c = \frac{q}{m} B_0. \tag{2.1}$$

In order to confine the particle in all three dimensions we superimpose a quadrupole electrostatic potential, generated by conductive electrodes (see figure 2.1), which makes the particle undergo a harmonic oscillator motion ("axial") *along* the z axis with frequency ω_z. Most modern precision Penning traps feature a cylindrical stack of electrodes. Even though the natural shape to produce a quadrupolar potential would be hyperbolic planes (with infinite size), the advantage of having open ends drastically simplifies ion transport as well as laser- and millimeter wave excitation. As the quadrupole potential necessarily causes a force in the x-y plane, the cyclotron motion splits into two new orthonormal modes, the "modified" cyclotron (with frequency ω_+) and the magnetron (with frequency

[1] In this thesis, ν denotes a frequency in Hz and $\omega = 2\pi\nu$ the respective angular frequency. In the text both will be called frequencies, in an effort to limit factors of 2π in the formulas.

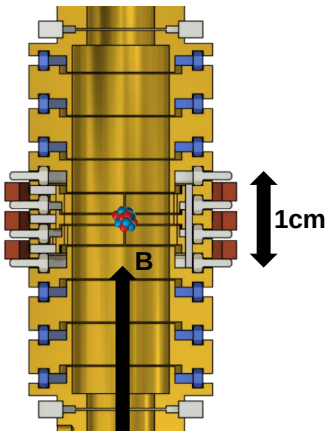

Figure 2.1: Cut-open view of a cylindrical electrode stack of the LIONTRAP precision trap. The axis of the cylinders is aligned with the magnetic field. The ion is confined in the center of the symmetric ring electrode. The inner electrodes are split to support radiofrequency excitations.

ω_-) motion. Typically, the frequencies show a clear hierarchy:

$$\omega_c > \omega_+ \gg \omega_z \gg \omega_-. \tag{2.2}$$

The trap eigenfrequencies, which are all dependent on the exact (and typically not sufficiently well known) properties of the trap electrode stack, can be combined to determine the "free" cyclotron frequency ω_c that depends solely on the magnetic field (and the particle properties):

$$\omega_c^2 = \omega_+^2 + \omega_z^2 + \omega_-^2. \tag{2.3}$$

This so-called invariance theorem [23] stays valid even in the presence of a number of unavoidable imperfections, such as a misalignment between the axis of the electric and magnetic fields and an elliptic deformation of the trapping field. Equation 2.3 is thus the basis for the precise determination of the magnetic field in a Penning trap. Without such imperfections, the frequency of the axial motion ω_z is defined by the strength of the electrostatic potential and the particle's charge-to-mass ratio:

$$\omega_z = \sqrt{\frac{qC_2V_0}{md^2}}. \tag{2.4}$$

Here, the unitless coefficient C_2, the voltage V_0 and the "characteristic trap dimension" d parameterize the strength of the harmonic part of the potential Φ. For hyperbolical traps d is connected to the ring radius, for cylindrical electrodes it has to be suitably chosen[2]. Its purpose is to make C_n unitless and consequently it always drops out in observables when used consistently. The general potential is defined in as Legendre series (consistent with the notation in [25], in the usual cylindrical coordinate system):

$$\Phi(r,\theta) = \sum_{n=0}^{\infty} \Phi_n = \frac{V_0}{2} \sum_{n=0}^{\infty} \frac{C_n}{d^n} r^n P_n(\cos\theta), \tag{2.5}$$

[2]For ALPHATRAP and LIONTRAP d has been calculated from the electrode lengths [24], alternatively one can choose it such that C_2 becomes unity.

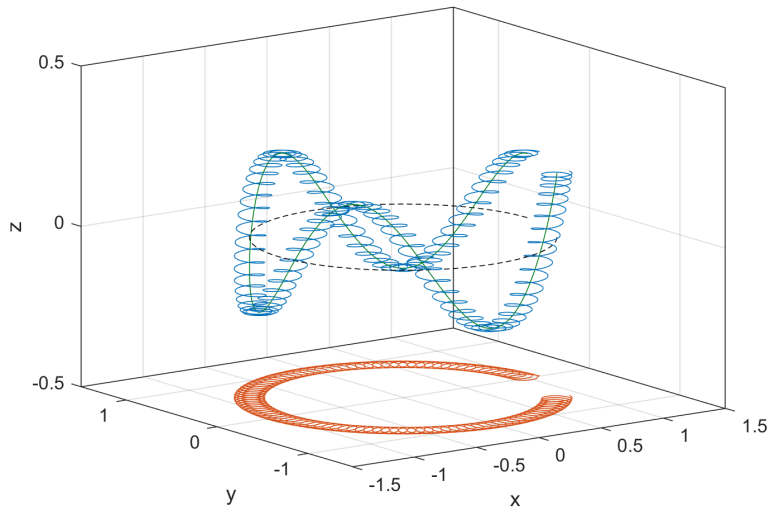

Figure 2.2: Motion of a particle in a Penning trap. The combined motion (blue) can be separated into the axial oscillation (green), the slow magnetron "drift" motion (black) around the electrostatic center and the rapid modified cyclotron oscillation. The red line is the projection on a constant-z plane. The amplitudes and frequencies are set to unusual values to improve the visualisation.

where the P_n are the Legendre polynomials. If the trap is designed in such a way that all $C_n > 2$ coefficients are negligible, the axial motion becomes harmonic and its stability depends solely on the voltage V_0. Since a constant voltage can be produced with much better stability than an alternating one, the motional frequencies in Penning traps are typically significantly better defined and less fluctuating than those in radiofrequency (rf) traps. Modern precision sources for constant voltages [26] can reach relative stabilities in the order of 30 ppb for minute timescales, translating into a 15 ppb stability of the axial frequency. In the future, the integration of Josephson junctions [**behr2012develop**, **ment**] to provide a reference voltage could even imprbetweene100 ppt and optimally this numbers. On that level, even the mechanical (in-)stability of the trap can cause comparable or larger fluctuations. The good temporal stability found in the most recent traps in turn allows us to tune out any residual anharmonicities in situ with the use of so-called correction electrodes to an extent where imperfections of the field are totally negligible at least for "cold" (comparable to 4 K) particles on small orbits. The largest frequency, ω_+, mostly depends on the magnetic field strength B_0. As the magnetic field is typically produced by a superconducting magnet in a stabilized environment, the relative stability[3] ${}^{\delta\omega_+}/_{\omega_+}$ can (and needs to) be significantly better than ${}^{\delta\omega_z}/_{\omega_z}$. Typically, between subsequent measurements a repeatability of between 100 ppt and optimally 30 ppt (in the case of LIONTRAP) can be reached. The same stability (on minute timescales) can be expected for all directly magnetic field dependent observables, such as e.g. the spin precession frequency. If the magnetic field is not perfectly homogeneous, the trap frequencies will generally depend on the orbit sizes. Similar as for the electrostatic potential, a series

[3] I use δ for fluctuations and Δ for nominal shifts.

expansion can be done for the axial component of the magnetic field:

$$B_z^{(n)} = B_n \sum_{k=0}^{\lfloor n/2 \rfloor} \frac{(-1)^k}{2^{2k}} \frac{n!}{(n-2k)!(k!)^2} z^{n-2k} \rho^{2k}. \tag{2.6}$$

The dominant terms are typically the lowest order even (in $n > 0$) terms. Since the particle oscillates mostly symmetrically with respect to the trap center, the odd order imperfections do not lead to secular frequency shifts in first order. In some cases however the combination of two odd order imperfections, such as $(C_3 \times B_1)$, B_1^2 or C_3^2 can cause sizeable effects. These will be covered in section 2.1.1.

2.1 Field imperfections

The field of the highly optimized precision traps used in our experiments are, for cold ions, extremely well described by the electrostatic quadrupole C_2 and the homogeneous magnetic field B_0. Magnetic inhomogeneities of the superconducting magnet have been minimized during the initial shimming of the magnet. Generally, the quadratic component B_2 of the magnetic field, the so-called magnetic bottle, causes an axial frequency shift proportional to the total axial angular momentum of the ion, which is mostly given by its cyclotron motion, but in parts also by its spin magnetic moment (if applicable). In the precision trap (PT) of ALPHATRAP and LIONTRAP the residual B_2 is quite small and can even be zeroed - in LIONTRAP with a specialised in-situ shim coil and in ALPHATRAP by shifting the trap position. In the analysis trap (AT) of ALPHATRAP however there is purposely a very large magnetic bottle. Here, we utilize the axial frequency shifts to to determine the spin state via the continuous Stern-Gerlach effect (CSGE, see chapter 2.4).

The lowest-order electrostatic anharmonicities C_4 and C_6 can be zeroed by applying the correct *tuning ratios* $\mathrm{TR}_{1,2}$, the voltage normalized to the ring voltage, to a set of two correction electrodes. The specific trap design makes sure that also the higher terms, C_8 and C_{10}, are very small. Consequently, once the tuning ratios have been optimized, the trap is harmonic even for millimeter-sized orbits (see figure 2.3) and certainly close to perfect for the typical micrometer-sized thermal amplitudes. However, by applying a slightly different tuning ratio we can purposely generate a specific, well-known C_4. In that case, all trap frequencies become dependent on the radii of the individual modes:

$$\begin{pmatrix} \Delta\nu_+/\nu_+ \\ \Delta\nu_z/\nu_z \\ \Delta\nu_-/\nu_- \end{pmatrix}_{C_4} = \frac{3C_4}{2C_2 d^2} \frac{1}{(\nu_+ - \nu_-)} \begin{pmatrix} \nu_- & -2\nu_- & 2\nu_- \\ (\nu_- - \nu_+) & (\nu_+ - \nu_-)/2 & (\nu_- - \nu_+) \\ -2\nu_+ & 2\nu_+ & -\nu_+ \end{pmatrix} \begin{pmatrix} \rho_+^2 \\ \hat{z}^2 \\ \rho_-^2 \end{pmatrix}. \tag{2.7}$$

When we set a well-defined C_4, we can accurately calibrate the mode radii by determining

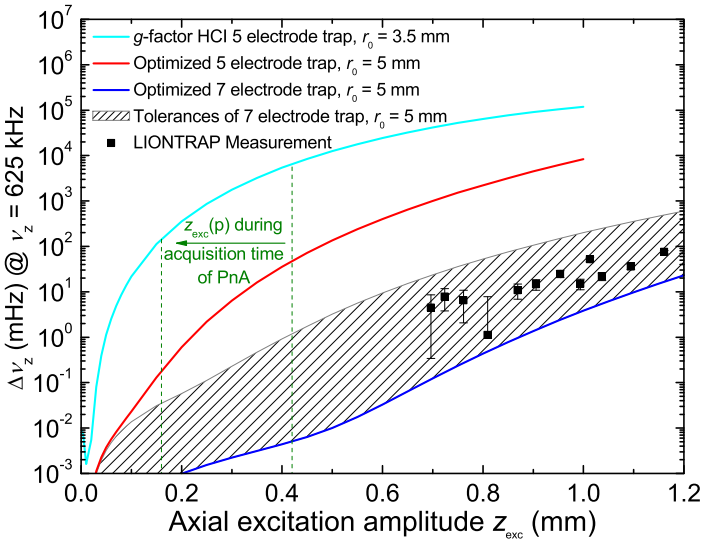

Figure 2.3: Simulated and measured axial frequency shifts resulting from the residual anharmonicities of different trap types. The hatched area shows the range predicted for the LIONTRAP PT, when allowing for manufacturing imperfections. The measured values are contained in that area and demonstrate a superior performance compared to previous designs and designs with only 5 active electrodes (one set of correction electrodes), rendering efficient phase-sensitive measurements of light ions possible. Figure taken from [22].

the frequency shifts. By repeatedly thermalising the ion and measuring its frequencies we can also accurately determine its energy distribution or "temperature". By previously exciting the ion with a well-defined dipolar excitation we exploit the quadratic radius dependence of the frequency shifts to attain drastically higher resolution especially if the ion is expected to be cold.

2.1.1 Odd order shifts

The mostly harmonic motion of the ion averages out any odd order field imperfections over full periods of the axial motion. However, the axial centroid shifts due to finite amplitudes and odd order field contributions. Figure 2.4 illustrates this effect at the example of a centroid shift due to finite axial amplitude, leading to a secular shift of the magnetic field in the presence of a residual magnetic gradient. Vice versa, the magnetic moment associated to the cyclotron rotation causes an axial force in the presence of a magnetic gradient. Generally, the lowest odd order shifts scale with the product of at least two odd order field imperfections and a squared radius, for example $C_3 B_1 \hat{z}^2$, $C_3 B_1 \rho_\pm^2$ or $C_3^2 \hat{z}^2$. These odd order shifts are particularly troublesome in the case of the coupled magnetron orbit method (see chapter 3.4.1), where we have nominally large magnetron radii. It is thus of importance to minimise the size of the odd order fields. For the magnetic gradient, this can be done via an in-situ shim coil. The C_3 contribution is a bit more problematic. Though it can in principle be zeroed with adjustments of the applied voltages, the unambiguous measurement of C_3 is difficult as it emulates frequency shifts very similar to a C_4. Zeroing the axial frequency shift after magnetron excitations does not necessarily lead to $C_3 = C_4 = 0$, but generally only cancels the individual shifts: $C_4 = \frac{3C_3^2}{4C_2}$. Instead, careful measurements of frequency shifts in more than one mode are required. Details on

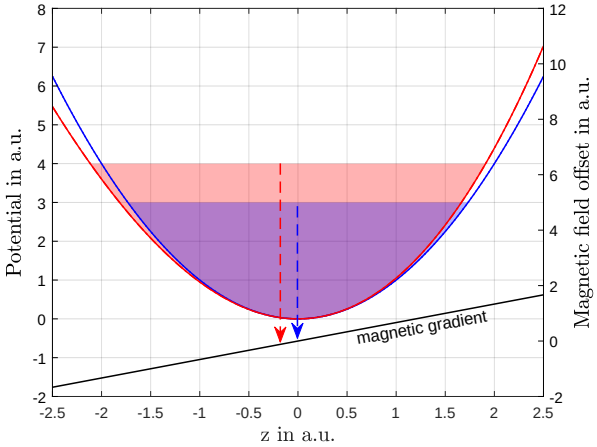

Figure 2.4: Shift of the mean axial position due to a $C_3 > 0$ (red) as function of the motional energy. The blue line shows a harmonic potential for reference. In first order the effective center of the motion shifts by $\Delta z \propto -C_3 \hat{z}^2$. In combination with a residual axial magnetic field gradient (black line), this position shift can cause secular frequency shifts.

this effect can be found for example in the PhD thesis of Dr. Sascha Rau [27].

2.1.2 Special relativity

The "ideal" Penning trap is characterized by the conditions $\Phi_{n>2} = 0$ and $B_{n>0} = 0$. However, eventually special relativity makes all motions non-harmonic. For the modified cyclotron and the axial motion this can be understood (in first order) as the relativistic mass increase, which makes the ion heavier with larger energy:

$$\left(\frac{\Delta\nu_+}{\nu_+}\right)_{\mathrm{sr}} \approx -\frac{E_+}{mc^2}. \tag{2.8}$$

By replacing E_+ with a thermal energy $k_B T_+$ we find a relative cyclotron frequency shift of about 0.1 ppt for medium-heavy ions without excitation. In a well-tuned trap the relativistic shift is actually the dominant anharmonic imperfection or if not cancelled by a suitably chosen magnetic bottle[4]. While 0.1 ppt seems small for cyclotron frequencies, the relative shift is about the same also for most optical transitions. Here, the effect is typically termed "second order Doppler shift". Consequently, for the ultra-high precision laser spectroscopy discussed in section 5, further cooling below the cryogenic environment is mandatory.

2.1.3 Image charge shift

In any real Penning trap, the harmonic potential is defined by a conductive electrode structure of necessarily finite size. The charged trapped ion then induces "image" charges into these electrodes. These charges move coherently with the ion and exert an attractive force onto it. In a cylindrical trap due to symmetry only in the radial direction there

[4]Such a cancellation can help to achieve less fluctuations during a measurement with finite temperature. However, it is only possible for one motion at a time and generally leads to additional shifts in the other modes.

is a sizeable force. Consequently, the magnetron and modified cyclotron frequencies are shifted with opposite sign. As there is no corresponding shift in the axial frequency, the invariance theorem yields a shifted cyclotron frequency. Generally, the image charge shift (ICS) has the form

$$\frac{\Delta\nu_c}{\nu_c} = \tilde{C}\frac{m}{4\pi\epsilon_0 B_0^2\,\rho_0^3} \tag{2.9}$$

where ρ_0 is the geometric radius of the trap and $\tilde{C}$ is a geometry factor that is unity for an infinite cylindrical trap. $\tilde{C}$ has been calculated numerically [28] for the geometry of LIONTRAP and ALPHATRAP. The uncertainty of the shift therefore results only from our finite knowledge of the geometric dimensions of the trap and is about 5% of the total shift. As the relative ICS scales linearly with the mass of the ion it is negligible when comparing mass doublets, but can reach ppb size for heavier ions. In LIONTRAP and even more in ALPHATRAP we have utilised the strong scaling with ρ_0^{-3} to reduce the ICS compared to previous trap generations, although the larger size has to be payed for with a lower signal level for the detection circuit. Specifically, the 9 mm ALPHATRAP PT results in only about 15 ppt uncertainty due to the ICS even for the heavy ^{208}Pb.

2.2 Ion detection and cooling

Since both LIONTRAP and ALPHATRAP are designed as versatile experiments with many different ion species to be targeted, also a versatile diagnostic method suitable for particles lacking optical transitions and capable of detecting single particles is required. The charged particle induces image charges onto the electrodes. Consequently, as the particle moves, the image charges generate radiofrequency currents at the trap frequencies that can be detected. To achieve sufficient voltage levels, a superconducting resonant tank circuit is used. When the frequencies of the trapped particle and the tank circuit coincide a sensitive cryogenic transistor amplifier can pick up the signal. As the image current flows through the tank circuit energy is dissipated and the particle eventually is cooled to the temperature of the tank circuit. At that temperature the thermal noise of the resonator offsets the dissipation and an equilibrium is established. The rate of this cooling is determined by the geometry of the trap and the charge and mass of the particle:

$$\tau = \frac{mD^2}{q^2 R}. \tag{2.10}$$

Here, D is the "effective electrode distance" of the plates of a notional parallel plate capacitor that would pick up the same image current as the detection circuit and can be accurately calculated with a finite element simulation. $R = Qw_R L$ is the resistance of the tank circuit in resonance, which can be increased by optimizing the quality factor of the

tank. For a superconducting axial tank circuit Q-values of about 40000 or even higher can be achieved, which then results in cooling time constants in the order of 50 ms. The axial and modified cyclotron motion can potentially be cooled with such a tank circuit, while the magnetron radius would increase indefinitely when energy is removed. Conveniently, the magnetron and cyclotron motion can be coupled to the axial motion via a radiofrequency sideband drive of suitable quadrupole "Q_{xz}" geometry[5]. If the axial motion is directly cooled by a tank, the sideband coupling causes the coupled motion to thermalise. The adiabatic coupling causes the expectation values of the quantum numbers of the coupled motions to equalize. Consequently, the temperatures become [29]:

$$T_{\pm} = \pm\frac{\omega_{\pm}}{\omega_z}T_z. \tag{2.11}$$

The magnetron temperature has a negative sign because the magnetron motion is so slow that the (negative) potential energy dominates its kinetic energy. The radiofrequency coupling to the axial motion is a very convenient method to cool arbitrary particles since the axial frequency can be made resonant with the axial tank circuit for every species simply by adjusting the trap voltage V_0. Compared to a direct cooling of the cyclotron motion with a dedicated tank circuit this convenience comes at the prize of a significantly higher temperature, as given in equation 2.11. Generally, T_z will be close to the temperature of the tank circuit, 4.2 K. Making use of the good noise properties of the cryogenic amplifier it is possible to feedback a fraction of the measured thermal noise with a suitable phase shift in order to partially cancel the thermal noise. Even though this reduces also the cooling rate, this method allows a significant reduction of the axial temperature. We have implemented this technique into our experiments and have observed minimum temperatures of about 1 K, consistent with expectations on basis of the observed signal-to-noise ratio [30]. Reaching even lower temperatures would require either a lower environmental temperature, for example via a dilution refrigerator, or superior amplifier technology, for example SQUIDs. In some cases it is feasible to furthermore lower the energy distribution of the ion by adiabatically (slowly) relaxing the trapping potential. In that case, while the occupied quantum numbers stay constant, the energy is reduced by a factor of $\omega_z^{\mathrm{initial}}/\omega_z^{\mathrm{final}}$ [17], at the cost that the axial frequency cannot longer be measured in that state and the trap center might have slightly shifted due to unavoidable imperfections in the trap. Significantly lower temperatures might become available in the future via sympathetic laser cooling (chapter 6.3).

[5] Q_{xz} denotes a two-dimensional quadrupole in the x-z plane.

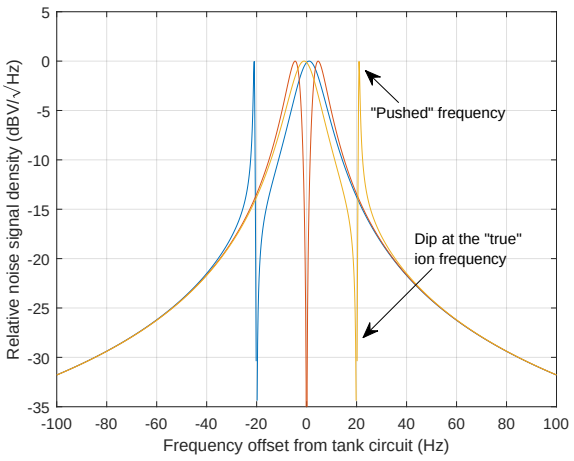

Figure 2.5: Noise resonance of the tank circuit and a thermalised ion. At the "true", unperturbed frequency of the ion, the noise density vanishes. If the ion is slightly detuned from the resonator, a dispersive lineshape with a maximum forms. The position of the maximum is subject to a "pushing" effect, which is contained in the theoretical lineshape, but leads to a systematic uncertainty.

2.3 Eigenfrequency determination

The tank circuit not only acts as a thermal bath, but also allows us to "listen" to the motion of the ion by detecting the image current. For excited ions, a Fourier analysis of the detected signal shows a narrow peak at the axial frequency ω_z of the ion if ω_z coincides (roughly) with the tank circuit resonance frequency ω_R. The peak has a finite width defined by the exponential cooling time constant τ_z and contains precise information on the frequency and phase of the ion motion. After some time, the ion is thermalised and the signal changes qualitatively.

2.3.1 The thermal noise dip

Now, as the ion will stay on a constant thermal amplitude over long times, there cannot be any signal left exactly at the frequency of the ion - otherwise the ion would be excited by this signal. Consequently, the image currents induced by the ion must exactly cancel the thermal noise of the tank circuit at ω_z and a "dip" in the detected noise density forms (see fig 2.5). The lineshape of this dip feature is well understood [22] and can be used to fit the detected spectrum and extract ω_z while the ion is at thermal energy. Consequently, systematic frequency shifts from trapping-field imperfections and special relativity are minimized in this case. On the downside, the relatively large linewidth makes the frequency readout prone to systematic errors and limits the statistical precision, especially because the signal is actually noise (or rather the absence of noise). Typically, after about a minute of sampling the ion's frequency can be determined to about 20 mHz, depending on the species and the quality of the detection system. While the frequency pushing effect resulting from the interaction of the tank circuit and the ion is accounted for in the lineshape model used for fitting, any departure from the theoretical lineshape will potentially lead to sizeable systematic shifts. If the ion is not exactly centered on

the resonator the imaginary part of the tanks circuit impedance leads to an asymmetric lineshape. Consequently, any symmetric fluctuation of the ion's frequency during the sampling time, as for example from fluctuations of the trapping voltages, will lead to a shifted fit result. While this specific effect is accounted for in our more advanced fitting procedures, further unknown effects can be present without our knowledge. Consequently, we specify a systematic uncertainty of about 20 mHz, or a bit less than one percent of the linewidth, for the absolute frequency, again depending on the combination of ion and detection system. In most experiments, only the axial motion can be directly determined with the tank circuit. In some specific cases, a dedicated resonator allows for the detection of the cyclotron motion, however this requires careful tuning of the tank circuit frequency for every ion species[6]. For this reason, the most commonly used technique to determine the remaining "radial" frequencies ν_+ and ν_- is based on the axial dip detection. To make the radial frequencies visible in the axial signal, we introduce a Q_{xz} radiofrequency drive at a frequency ν_d close to the respective axial sidebands $\nu_d = \nu_+ - \nu_z$ and $\nu_d = \nu_z + \nu_-$. Now, the axial and radial modes periodically exchange motional amplitude with a "Rabi" frequency controlled by the strength of the drive. Consequently, the axial motion is now amplitude modulated, and the frequency spectrum shows a split line or a "double dip" once the motion is thermalised. This is equivalent to the spectrum of the dressed axial state following from the AC-Stark splitting by the drive. If the drive coincides exactly with the sideband frequency, the double dip is symmetric with respect to the (now invisible) single axial dip. If there is a slight detuning, we can determine the true sideband frequency from the measured double-dip frequencies ν_l and ν_r via the relation

$$\nu_\pm = \nu_d \pm (\nu_l + \nu_r) \mp \nu_z. \tag{2.12}$$

This way, by alternately measuring the double-dip and single-dip frequencies, all eigenfrequencies can be determined. However, while this technique is very versatile and robust to use, the precision and accuracy with which the dip frequencies can be extracted imposes a stringent limitation.

If the ion is excited above the thermal energy of the resonator it appears as a peak rather than a dip. In this situation not only the signal is larger, but it becomes possible to read the coherent phase of the ion motion. This is the basis for a number of phase-sensitive measurement techniques, which allow for superior precision compared to dip-based methods. Here, I will briefly introduce the basics of the most frequently used techniques, the frequency estimation with direct peak detection and the phase-sensitive techniques Pulse-and-Phase (PnP) and Pulse-and-Amplify (PnA). More detailed information can be found in the respective original publications, specifically [29, 31] and from our group:

[6]While the axial frequency can be tuned by applying suitable trap voltages, the modified cyclotron frequency is mostly dependent on the magnetic field, which cannot be easily adjusted.

- Phase-sensitive cyclotron frequency measurements at ultralow energies

  S. Sturm et al. "Phase-sensitive cyclotron frequency measurements at ultralow energies". In: *Phys. Rev. Lett.* 107.14 (2011), p. 143003

and

- g-factor measurement of hydrogenlike $^{28}Si^{13+}$ as a challenge to QED calculations

  S. Sturm et al. "g-factor measurement of hydrogenlike $^{28}Si^{13+}$ as a challenge to QED calculations". In: *Phys. Rev. A* 87.3 (2013), p. 030501.

2.3.2 Direct peak detection

This technique requires a detector that allows a continuous detection of the image current of the respective mode. This is typically the case for the axial motion, but rarely for the cyclotron motion, mainly because until today there is no proven technique that allows tuning a high-Q resonator over a sufficiently large range to cover the cyclotron frequencies of different ion species. Consequently, a cyclotron resonator has to be custom-built for every ion type. The detected signal can typically be modeled as a coherent, exponentially damped sinusoidal signal on a white noise background. The damping with a time constant τ, typically originating from dissipation of the image current on the resonator, leads to a Lorentzian lineshape with a natural linewidth of $\Gamma = \frac{1}{2\pi\tau}$. Additionally, temporal instabilities in the measured frequency, originating mainly from magnetic and electric field fluctuations, can lead to sizeable line-broadening especially if the damping is slow. For the axial frequency the damping is typically strong and dominates the linewidth if the ion is resonant with the detector, while for the cyclotron frequency typically the magnetic field fluctuations are larger than the natural linewidth. As long as the measurement or data acquisition time is short compared to the time-scale set by these fluctuations, the ideal precision of the frequency estimation can be calculated with the Cramér-Rao lower bounds:

$$\delta\nu = \sqrt{\frac{12\pi}{\omega_s^3\,\mathrm{SNR}\,T^3}}, \tag{2.13}$$

where ω_s denotes the sampling frequency and SNR is defined as the signal-to-noise ratio at that sampling rate. This shows that the achievable precision scales very favourably $\propto \frac{1}{\sqrt{T^3}}$ in this regime. In order to make use of the ideal precision given by the Cramér-Rao lower bounds [34] via a Fourier transform, suitable amounts of zero-padding [35] can be used.

2.3.3 PnP and PnA

The phase-sensitive techniques PnP and PnA are the methods of choice in most modern cryogenic Penning-trap experiments. They allow measuring the cyclotron frequency of

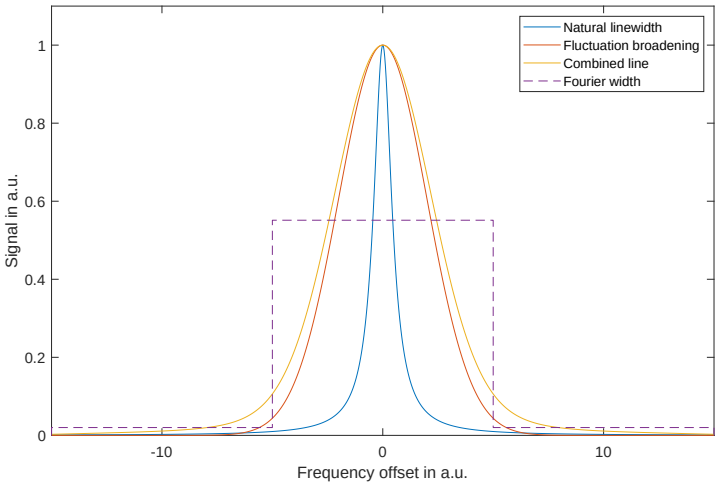

Figure 2.6: Lineshape of the detected cyclotron amplitude signal. The natural linewidth (blue) due to the resistive cooling with timescale τ_+ can be much smaller than the Fourier width (purple, dashed), which is given by the inverse measurement time. Magnetic field fluctuations within the detection time lead to further broadening (red) and result in a combined line (yellow).

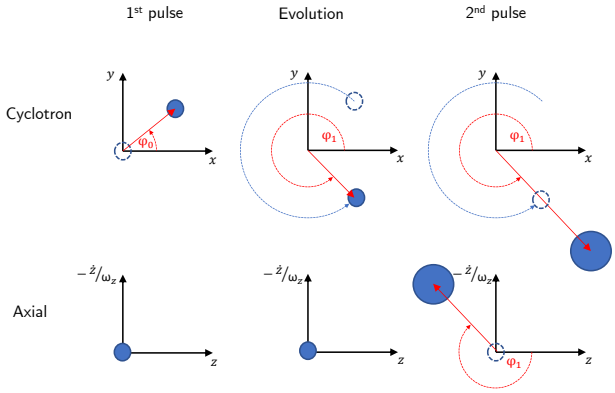

Figure 2.7: PnA sequence. The first pulse at ω_+ excites the ion to a cyclotron orbit with phase φ_0. Afterwards, the ion freely evolves until it reaches the phase ϕ_1 after some time T_{evol}. Finally, a second pulse on the blue axial sideband at $\omega_+ + \omega_z$ causes a parametric amplification and consequently a transfer of the cyclotron phase information onto the axial motion, from where it is determined via a Fourier transform.

most ions in the absence of a cyclotron detector. To this end, they imprint a phase φ_0 onto the cyclotron motion and then let the motion evolve freely. Eventually, after some "evolution time" T_{evol}, the final phase $\varphi_1 = \varphi_0 + \omega_+ T_{\text{evol}}$ is detected by transferring the phase information to the axial motion, where it can be detected via the axial tank circuit. This way, even in the presence of (reasonably small) temporal fluctuations the almost exact mean of the magnetic field $\langle B(t) \rangle$ is determined:

$$\varphi_1 = \varphi_0 + \int_{t_0}^{t_1} \omega_+(t) \mathrm{d}t \overset{\substack{\text{ideal trap \&} \\ \text{small fluctuations}}}{\approx} \varphi_0 + \left(\frac{q}{m} \langle B(t) \rangle - \omega_- \right) T_{\text{evol}}. \tag{2.14}$$

As the phase φ_1 can be only measured modulo integer 2π rotations, it is necessary to "unwrap" the total phase by measuring with different, suitably chosen T_{evol}. For this to work, the prediction of the phase for the next longer T_{evol} has to be significantly better than π. This sets a natural limit for T_{evol}, as magnetic field fluctuations finally lead to excessive shot-to-shot fluctuations. For current-generation traps this time is typically below one minute for $\frac{q}{m} \approx \frac{e}{2u}$. The precision of the frequency determination depends on

the standard deviations of the initial ($\delta\varphi_0$) and final ($\delta\varphi_1$) phases and their determination:

$$\delta\nu = \frac{\sqrt{\delta\varphi_0^2 + \delta\varphi_1^2}}{2\pi T_{\text{evol}}}. \tag{2.15}$$

For HCI[7] we can typically achieve $\delta\varphi_1 < 10°$, while $\delta\varphi_0$ can be made almost arbitrarily small by repeated measurements. Consequently, the frequency uncertainty for a single measurement can reach $\delta\nu < 1\text{mHz}$, which corresponds to a fractional precision of about $\frac{\delta\nu_+}{\nu_+} \approx 40\,\text{ppt}$ for the cyclotron frequency (at about 20 s evolution time). The measured phase and its precision represents the real frequency, including all relevant shifts. So if the magnetic field fluctuates, φ_1 measures the mean magnetic field $\langle B\rangle$ during the evolution time with high precision, however at the time of a second measurement this field will have changed to some extent. The impact of these fluctuations in between successive measurements will be discussed in chapter 3.

2.4 The continuous Stern-Gerlach effect

The image current detection enables us to measure all motional eigenfrequencies of virtually arbitrary ions. However, in order to get access to the state and precession frequency of the spin a different tool is required. If there are optically accessible transitions available in the ion, there are several well-established techniques that typically rely on the detection of fluorescence photons. In a Penning trap however, there is a very elegant and extraordinarily versatile method that does neither require driving any internal transition nor detecting fluorescence. Hans Dehmelt originally pioneered using the Stern-Gerlach effect inside a magnetic bottle to detect the spin-state of electrons [5]. By making the magnetic field inside a Penning trap deliberately inhomogeneous, any magnetic moment associated with the trapped ion experiences a force. However, not only the internal spin and orbital angular momentum contributes to μ_z, but also the energy in the cyclotron and magnetron motion:

$$\mu_z = \mu_z^{\text{l,s}} + \frac{2q}{m\omega_+}\left(E_+ - \frac{1}{2}E_-\right). \tag{2.16}$$

While the magnetron energy is typically negligible in this context, the contribution of the cyclotron motion is typically[8] one or two orders of magnitude larger than $\mu_z^{l,s}$. If the inhomogeneity is quadratic along the axial direction, the force is harmonic: $F_z = \mu_z \nabla_z B(z) = 2B_2\mu_z z$. This additional force thus leads to an axial frequency shift depending

[7] This is not quite true for the lightest ions, such as the proton, where the low mass leads to large relativistic shifts and the low charge results in low signal strength.

[8] For an internal magnetic moment in the order of a Bohr magneton and a resisitvely cooled ion.

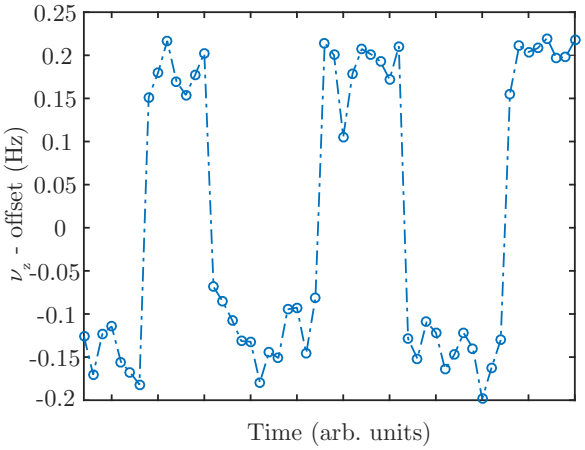

Figure 2.8: Determination of the spin orientation of a $^{40}Ar^{13+}$ ion in ALPHATRAP. The axial frequency is continuously monitored via the noise dip. In between the measurements mmW are injected, which potentially change the ion's Zeeman sublevel. In that case, the axial frequency jumps instantaneously by about 330 mHz. This figure is taken from the PhD thesis of Dr. Ioanna Arapoglou [36].

on the magnitude and sign of the total magnetic moment μ_z:

$$\Delta\nu_z \approx \frac{\mu_z B_2}{4\pi^2 m \nu_z}. \tag{2.17}$$

For s-state ions, the spin part of μ_z is always on the order of a Bohr magneton. Consequently, the axial frequency jump $2\Delta\nu_z$ is proportional to $1/m$, so that the requirement on the relative stability of the trap voltage increases for heavier ions. Then again, the shift due to the motional angular momentum also decreases with m, so that even for hydrogen- or lithiumlike $^{208}Pb^{81+}$ the $2\Delta\nu_z \approx 150$ mHz frequency jump can be unambiguously resolved. Figure 2.8 shows an exemplary sequence of spinflips for the comparable case of boronlike argon, where the magnetic moment is about $\mu_B/3$ due to the Landé g_j-factor of the $p_{1/2}$ groundstate. This demonstrates that the CSGE allows us to determine the current Zeeman substate even for the heaviest ions, as long as $g_j \gtrsim 0.5$.

3 | Mass measurements of the lightest elements

The atomic masses of the lightest isotopes, the proton, deuteron, triton, ^{3,4}He and the electron are of special importance for precision experiments in atomic and nuclear physics. They are required to interpret the spectra of atomic hydrogen, the hydrogen molecule and the molecular hydrogen ion and its isotopologues. Today, extremely precise measurements of these spectra are available and the comparison of the measured transition frequencies with their theoretical predictions allow unique tests of our understanding of physics. In fact, no individual mass enters these calculations but always unitless ratios, such as for example the proton-to-electron mass ratio. Consequently, the measurement unit is in principle arbitrary for this purpose. However it is customary to refer atomic masses to the atomic mass unit u, which is defined as $1/12^{\text{th}}$ of the mass of a ^{12}C atom[1]. Also the electron mass has been measured directly in units of the ^{12}C mass. Over the last years, my group has measured these fundamental mass values:

- Electron atomic mass to 28 ppt via the magnetic moment of $^{12}C^{5+}$:

  S. Sturm et al. "High-precision measurement of the atomic mass of the electron". In: *Nature* 506.7489 (2014), pp. 467–470

- Proton atomic mass to 32 ppt:

  F. Heiße et al. "High-precision measurement of the proton's atomic mass". In: *Phys. Rev. Lett.* 119.3 (2017), p. 033001

- Deuteron atomic mass to 8 ppt (most precise atomic mass measurement):

  S. Rau et al. "Penning trap mass measurements of the deuteron and the HD^+ molecular ion". In: *Nature* 585.7823 (2020), pp. 43–47

An overview on these measurements is given in the following chapters, further information can be found in our publications, which are part of this thesis.

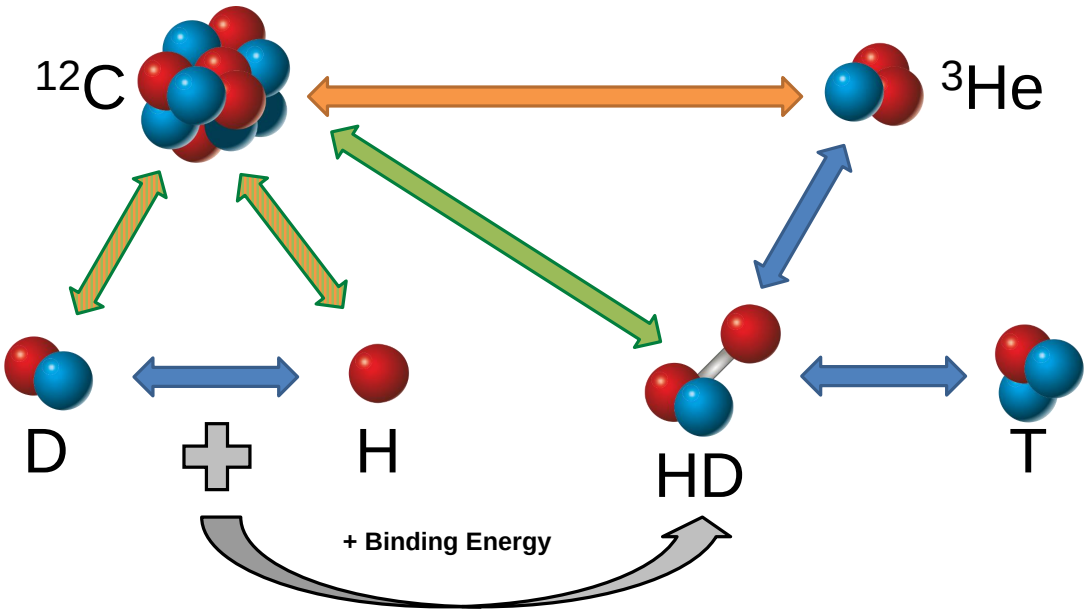

Figure 3.1: Light ion mass puzzle. The masses of the lightest elements are connected by a series of ratio measurements performed by different leading groups: orange: van Dyck / UW, blue: Myers / FSU, green: Sturm / MPIK. The measurements are redundant and a significant discrepancy is found. Our measurements have revealed problems in the UW data while the FSU/MPIK data are in excellent agreement. The remaining link between ^{3}He and ^{12}C has only been measured by UW and will be targeted in an upcoming campaign of our group.

3.1 The light ion mass puzzle

Over the last decades a number of setups have contributed at relevant precision to the mass values tabulated by the CODATA group of the National Institute of Standards and Technologies (NIST [40]) and the evaluation of atomic masses (AME, [41]). Among them are the now discontinued SMILETRAP setup in Stockholm and the Penning-trap setup of Prof. R. S. Van Dyck Jr. at the University of Washington (UW-trap) as well as the former MIT-trap that has been moved to the lab of Prof. Dr. Edmund G. Myers at Florida State University (FSU-trap) and our LIONTRAP setup. When the mass difference of the HD^+ molecular ion and $^3He^+$ was measured at FSU-trap in 2015 [42] a second, redundant link between the masses of proton [43] and deuteron [44] and the ^{3}He mass [44] was established. By comparing the atomic mass of the HD^+ molecule determined from the masses of the constituents and their respective binding energy to the one linked via ^{3}He to u, a discrepancy of 4.4 standard deviations ("σ") became apparent (the "light ion mass

[1]Since the new definition of the SI units in 2019 the Avogadro number N_A has a defined value and so $12N_Au$ is not anymore exactly 12 grams.

puzzle" (LIMP), see figure 3.1). Obviously, in the light of the importance of accurate, high-precision mass values of these ions, such a tension leaves unacceptable doubts on the reliability of the Penning-trap measurements. This motivated us to develop LIONTRAP specifically to perform dedicated high precision measurements of light ion masses directly versus $^{12}C^{6+}$. The first campaign targeted the proton mass [38], where indeed we found a 3σ deviation to the tabulated value. When using the LIONTRAP value for the proton mass, the total LIMP discrepancy was reduced to 3.5σ. Later, a remeasurement of the HD^+ to ^{3}He link in the FSU-trap yielded a consistent, yet more precise result, so that while the absolute discrepancy was not significantly altered, the significance was increased again to 4.8σ. We used our experience from the proton mass campaign to develop several technical improvements for LIONTRAP:

- An **in-situ shim coil** that allowed us to drastically reduce the magnetic inhomogeneity that had previously been the dominant source of systematic uncertainty
- An **angle adjustment system** that allows us to null the angle between the electrostatic and magnetic trap axis
- A **pressure stabilization** system for the liquid helium and liquid nitrogen tanks.

In the following campaign, we were able to determine the atomic mass of the deuteron with world-leading precision. Again, our result differed from the UW value, this time by 4.8σ, while the proton-to-deuteron mass ratio that we can extract from our two campaigns agrees with a recent direct determination at FSU-trap [45] on a 1σ level. With our values, the LIMP reduces to 3σ. Recently, high-precision laser spectroscopy results on ro-vibrational transitions in HD^+ became available [20, 46, 21]. These transitions are sensitive to a combination of the constituent masses of the molecule:

$$f \propto m_e \left(\frac{1}{m_d} + \frac{1}{m_p} \right). \tag{3.1}$$

Consequently, the laser spectroscopy results can be compared to the results from our cyclotron frequency measurements of m_p and m_d and our determination of the electron mass from the magnetic moment of hydrogenlike $^{12}C^{5+}$. These results also agree on a 1σ level, which not only strongly supports and confirms the set of mass values determined by LIONTRAP and FSU-trap, but also validates QED in medium strong fields as well as in molecules. Consequently, we assume that the remaining tension of the LIMP will be found in the ^{3}He-to-^{12}C ratio, which has up to now only been measured by the UW group to relevant precision. This measurement will be target of a future campaign of LIONTRAP.

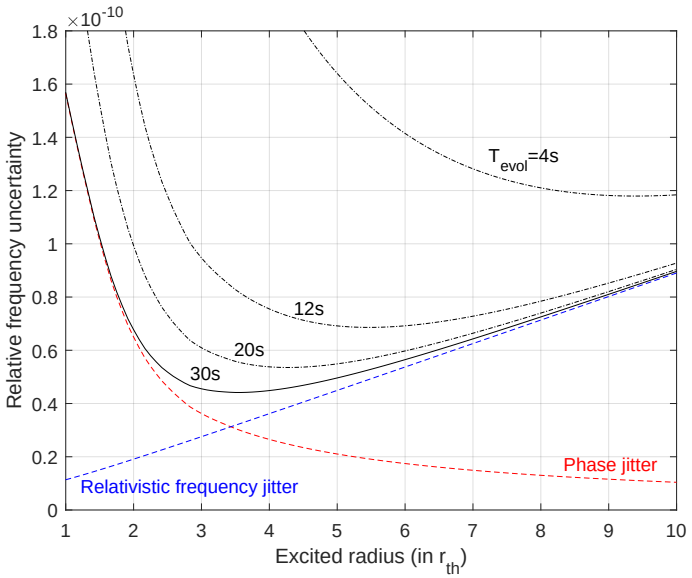

Figure 3.2: Single-shot cyclotron frequency precision due to phase definition jitter and relativistic frequency shift as function of the chosen excitation strength for a proton in LIONTRAP. Minimal uncertainty is reached for the longest evolution times.

3.2 Specific challenges for light ions

Reaching high precision with light ions brings some specific challenges. Firstly, the low charge means the detectable signal strength is low for a given oscillation amplitude, especially if the trap size is chosen large in order to limit the image charge effect. Since most shifts of the trap eigenfrequencies depend on the oscillation amplitude, the trap should consequently be extraordinarily harmonic and the image current detector needs to be extraordinarily sensitive. The novel design of LIONTRAP guarantees that even for the most problematic candidates, such as singly charged protons, deuterons or $^3T^+$, the frequency shifts stay low enough to allow phase-sensitive measurements. On the other hand, the thermal radius in equilibrium with a fixed (axial) tank circuit at a given temperature scales inversely to the mass:

$$\hat{z}_{th} = \sqrt{\frac{2k_B T_z}{m\omega_z^2}}. \tag{3.2}$$

The dominant systematic frequency shifts due to magnetic field inhomogeneities and particularly special relativity (see e.g. equation 2.8) scale with the motional amplitudes squared $\Delta\nu/\nu \propto \hat{r}^2$. Moreover, for phase sensitive measurements the amplitude after excitation has to significantly surpass the thermal radius to allow for a good phase precision. This means that a very homogeneous magnetic field is mandatory for light ion mass measurements, but ultimately the shifts by special relativity can only be counteracted by a low ion temperature. At LIONTRAP we made sure to prevent any excess heating from external noise or the detection amplifier from elevating the equilibrium temperature above the 4.2 K of the cryogenic bath. Additionally, electronic noise feedback (chapter 2.2 and

ref. [30]) is routinely used to lower the ion's axial temperature below 4.2 K. In the current electronic setup the minimum axial temperature achievable in this way is slightly below 1 K. This is sufficient to support mass measurements in the ppt regime even for light ions, especially if relatively long evolution times can be used. Figure 3.2 shows the achievable single-shot precision for a proton in LIONTRAP if only the phase precision after excitation and the relativistic frequency shift is considered. For heavier HCI, the precision can be significantly higher.

3.3 Penning-trap mass ratio measurements

Masses are measured in Penning traps by determining the ratio of cyclotron frequencies ("CFR") of two ions. Normally, only a single ion is in the trap at any time, which is then swapped regularly with the second ion and the cyclotron frequencies are measured alternately. Here, the main assumption is that the ions a and b on average see exactly the same magnetic field - only then we can assume that the magnetic field drops out in the ratio of cyclotron frequencies $\mathrm{CFR}_{a,b}$

$$\mathrm{CFR}_{a,b} = \frac{\left\langle \nu_{c(a)} \right\rangle}{\left\langle \nu_{c(b)} \right\rangle} = \frac{q_a m_b}{q_b m_a} \frac{\langle B_a \rangle}{\langle B_b \rangle} \stackrel{!}{=} \frac{q_a m_b}{q_b m_a}. \tag{3.3}$$

If one of the ions has a known mass (or is a ^{12}C ion), the measurement of $\mathrm{CFR}_{a,b}$ relates the other one to the atomic mass unit if we assume that q_a/q_b is a known integer. This procedure implies that the ions have to be located at exactly the same spot at slightly different times, one after the other (see fig. 3.3). Consequently, there will be excess fluctuations of ν_+ depending on the stability of the magnet on the relevant time-scale, which average out over many measurement cycles, especially if the order of measurements is randomized to suppress linear field drifts. If the two ions have significantly different axial frequencies, a measure has to be found to bring each ion into resonance with the tank circuit. Although this can trivially be done by adjusting the trap voltage, in that case it is easily possible to inadvertently shift the spatial trap center slightly. Typically, trap electrodes carry so-called "patch potentials", a combination of trapped surface charges and varying work functions of the electrode surface. These extra potentials are rarely below about 10 mV and not necessarily homogeneously distributed. This causes the center of the electrostatic potential to slightly depart from the geometric center of the trap. If the applied voltages are changed, the impact of the patches changes and consequently moves the electrostatic field center. As the magnetic field in any real trap is only imperfectly homogeneous, such a shift will cause a systematic discrepancy of $\langle B_a \rangle$ and $\langle B_b \rangle$ that is difficult to quantify. However, to give an illustrative example, let us assume the patch potentials in our (otherwise ideal) trap produce a constant linear potential gradient

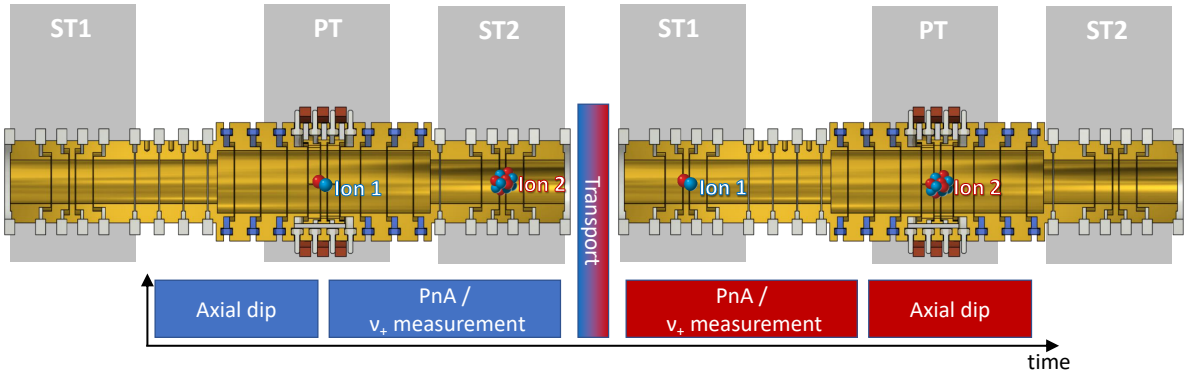

Figure 3.3: Typical cyclotron frequency ratio (CFR) measurement sequence. Both ions of interest are stored simultaneously, but in separate traps. By transporting them alternatively to the same position in the precision trap (PT), the time between the relevant cyclotron frequency measurements can be minimized. The other ion is meanwhile stored in one of the storage traps (ST1 and ST2). Each cycle a random generator decides which ion is measured first, so that systematic effects associated to drifts are cancelled.

$k_{\mathrm{pp}} \approx 2\,\mathrm{mV\,mm^{-1}}$ along the axis: $\varphi = k_{\mathrm{pp}}\,z + \frac{C_2 V_0}{2\,d^2} z^2$. The minimum of φ thus shifts by $\Delta z = \frac{d^2\,k_{\mathrm{pp}}}{C_2\,V_0}$, or, for small voltage changes: $\Delta z \approx -\frac{d^2\,k_{\mathrm{pp}}}{C_2\,V_0^2}\,\Delta V \approx -13\,\mu\mathrm{m}\frac{\Delta V}{V_0}$. This last estimation means that for ions with largely different q/m these patch potentials would typically cause totally unacceptable systematic shifts in the ppb regime[2]. For good q/m doublets this effect is largely suppressed due to the small ΔV, but stays a critical contribution for the 11 digits precision level.

A much better technique adjusts the detector frequency to the ion rather than the ion to the detector. For relatively small adjustments, as necessary for isobars ($\frac{q}{m}$-doublets) this can be done with the help of an electronically controlled capacitor (varactor) that changes the resonance frequency of the tank circuit. For larger changes in $\frac{q}{m}$ a second independent detector is required. The latter has been realized in LIONTRAP for our proton mass campaign, where the mismatch of the charge-to-mass ratios of the ion of interest (the proton) and the reference ion (hydrogenlike carbon $^{12}C^{6+}$) was a factor of two. There, one detector at relatively high and fixed frequency was dedicated to the proton, while a second detector has been carefully tuned to the frequency of the $^{12}C^{6+}$ ion. While the choice of one detector frequency (ν_{R1}) is largely free as we can adjust the trap voltage accordingly, the second detector frequency (ν_{R2}) automatically has to match the ratio of charges and masses: $\frac{\nu_{R1}}{\nu_{R2}} \stackrel{!}{=} \sqrt{\frac{q_1 m_2}{q_2 m_1}}$, as we do not want to change the trap voltage during the campaign. This is a significant practical complication, since the superconducting detector frequency cannot easily be measured at room-temperature and also changes by roughly one percent

[2]Assuming a magnetic gradient of about $\mathrm{mT\,m^{-1}}$

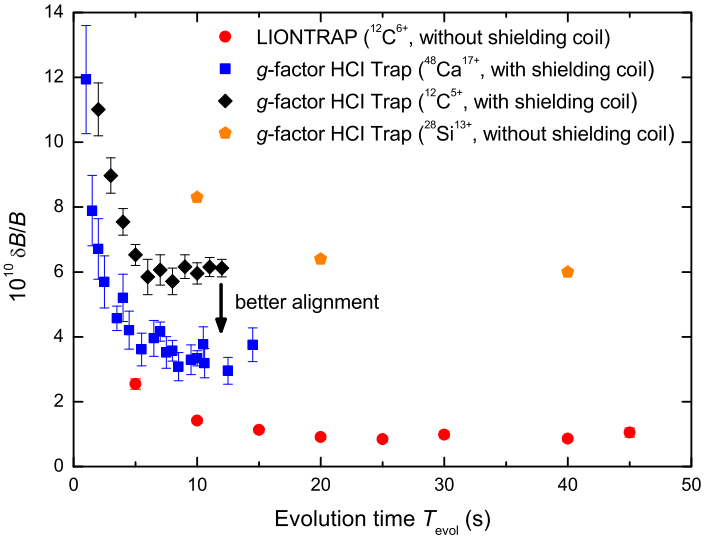

Figure 3.4: Shot-to-shot fluctuation of the modified cyclotron frequency in LIONTRAP, compared to our previous setup that contained a ferromagnetic ring (compare also chapter 4), but also a superconducting self-shielding coil. The optimal precision, better than 100 ppt per shot, is reached for evolution times of about 30s. For significantly longer times phase-coherence is lost. Figure taken from [22].

when cooled down. Still, by using a varactor for fine-tuning in-situ we have successfully implemented a matching pair of detectors that consequently allowed totally avoiding the systematic uncertainty associated to shifts of the trap center and allowed reaching beyond state-of-the-art precision for the proton mass [38]. For the later deuteron mass campaign [39] the varactor alone was sufficient to tune one detector alternatively to the deuteron and the carbon thanks to the close matching of these charge-to-mass ratios. For this campaign we have significantly improved the stability of the environmental parameters such as the pressures in the cryostats and the temperature of the apparatus, resulting in a better temporal stability of the magnetic field (see fig. 3.4) and consequently allowing us to perform the most precise mass measurement in atomic mass units to date with an accuracy of 8 ppt. While obviously further incremental technical improvement should and will happen, at this point we are starting to see the impact of many different small sources, making significant progress very difficult.

3.4 Simultaneous measurements

To generally circumvent excess magnetic field fluctuations, different techniques have been developed with varying success. In a stack of several traps it is possible to prepare two or more single ions in individual potential minima (see figure 3.3). This way, after each measurement the ions can be exchanged significantly faster than in a single trap, where the ions have to be either produced and killed successively or one ion has to be parked on a large orbit [47]. By sandwiching the most relevant phase sensitive measurements with the less critical ones, the time scale relevant for magnetic field fluctuations can be drastically reduced. However, practically this "rapid transport" technique is limited by the settling times of the trap voltages after transports. The precision voltage sources suffer

from minute-scale drifts after the voltages have been changed, which forces us to include waiting times in between the precision measurements. To circumvent this we are currently building a dedicated transport voltage source, which performs the transports and allows the precision sources to keep their output constant. We expect a significant reduction of the wait times and a correspondingly large improvement of the achievable precision, however the effect of the cryogenic filters still has to be thoroughly analyzed once the new source becomes operational.

In LIONTRAP we have two separate traps both equipped with their own detector. This allows us to perform truly simultaneous measurements on two ions. While the absolute magnetic field in the two traps slightly differs due to the spatial distance, we expected the fluctuations to be largely the same. By storing two ions of interest and additionally a reference ion in the trap stack, we can alternatively measure the cyclotron frequencies of one ion with respect to the reference ion and then afterwards measure the other ion also with respect to the same reference ion. This way, since both measurements measure the ions of interest simultaneously with the reference ion, the ratio of both results should yield the ratio of the cyclotron frequencies of the ions of interest with high precision, while the reference ion drops out. The time-dependent magnetic field in the "precision" trap (a) can be written w.l.o.g. in terms of the field in the reference trap (b), the constant field offset $\Delta B_{a,b}$ and the time variation of the field offset $\delta\Delta B_{a,b}(t)$:

$$B_a(t) = B_b(t) + \Delta B_{a,b} + \delta\Delta B_{a,b}(t). \tag{3.4}$$

Since the phase sensitive measurements determine the mean magnetic fields, the ratio of the measured fields and consequently the determined cyclotron frequencies[3] become

$$R \equiv \frac{\nu_c^a}{\nu_c^b} = \frac{q_a m_b}{q_b m_a} \frac{\langle B_a(t)\rangle}{\langle B_b(t)\rangle} = \frac{q_a m_b}{q_b m_a}\left(1 + \frac{\Delta B_{a,b}}{\langle B_b\rangle} + \frac{\langle \delta\Delta B_{a,b}\rangle}{\langle B_b\rangle}\right). \tag{3.5}$$

If the field fluctuations commonly influence both traps, $\delta\Delta B_{\mathrm{a,b}}$ will be small and R becomes largely time independent. However, to our surprise at least in the LIONTRAP setup $\delta\Delta B_{\mathrm{a,b}}$ actually dominates (the fluctuations are mostly independent in the two traps) on the relevant time scales and consequently the method does not improve precision as expected. In the future a thorough analysis of the sources of the individual fluctuations is required to eventually bring the two-trap method to success.

3.4.1 Coupled magnetron orbits

A quite different method has originally been pioneered at MIT in the Pritchard group [48]. Here, the two ions of interest are simultaneously stored in the same trap. It is based on

[3] For the sake of clarity I neglect the minute difference of ν_+ and ν_c here.

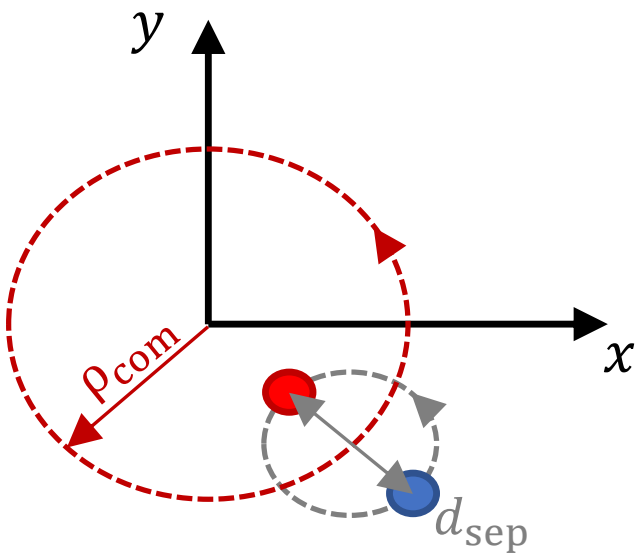

Figure 3.5: Coupled magnetron orbit. Two ions stay on an (almost) constant distance d_{sep} and circulate around their common guiding center. The guiding center rotates around the trap center on an (almost) constant radius ρ_{com}. By making ρ_{com} small, the two ions sample on average the identical magnetic field and effectively exchange position every magnetron half-cycle. Consequently, the cyclotron and spin precession frequencies stay (relatively) coherent even for very long evolution times.

the observation that the magnetron frequency ν_- is in first order independent on the ion charge-to-mass ratio. If the charge states and masses of the ions are similar and the axial motions are cold, the minute second-order mismatch in ν_- is overcome by the Coulomb interaction and the magnetron motion becomes coupled. In this state, the two ions perform rotations both around themselves as well as around the trap center (see figure 3.5).

With a sequence of radiofrequency excitations ρ_{com} can be reduced until the ions circulate basically only on d_{sep}. In this state the ions are not only very close together, but on average sample the identical magnetic field (for identical ions) and exchange position every magnetron half-cycle. Consequently, any magnetic field fluctuation that is homogeneous on a scale of a few hundred micrometer (the typical scale for d_{sep}) are perfectly canceled. In fact, even non-homogeneous fluctuations that are slower than the magnetron frequency cancel to a large extent. This is especially important in the case of the spin precession frequency. A homogeneous magnetic field excursion ΔB that is seen by one ion w.r.t. the other for a time $t < \frac{\pi}{\omega_-}$ causes a deviation of its spin precession or respectively cyclotron phase by $\Delta\varphi_{L,+} = \omega_{L,+}\frac{\Delta B}{\langle B_0\rangle}t < \pi\frac{\omega_{L,+}}{\omega_-}\frac{\Delta B}{\langle B_0\rangle}$. While this phase jitter is typically negligibly small for the cyclotron motion, for the much larger spin precession frequency it could sum up to problematic values over the total measurement time. Luckily, the electric conductivity of the trap material and the surrounding seems to effectively shield such high frequency field fluctuations and first measurements clearly proof the concept. As the impact of magnetic field fluctuations is now effectively excluded, other effects shift into focus. First of all, any differential frequency shift between the ions obviously does not drop out. This includes shifts due to special relativity. Since both ions are only cooled to finite temperature in our setups, already in the thermal state there

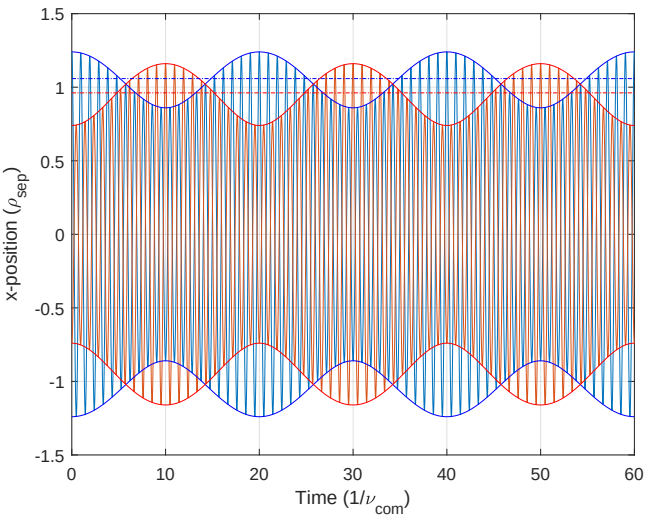

Figure 3.6: Magnetron-like orbits of the coupled ions (red and blue) along the arbitrarily chosen x direction. The relatively fast magnetron oscillation is modulated at the difference of separation- and common frequencies. Due to the imperfect matching of the ion masses, the common- and separation amplitudes are not perfect constants of motion. Consequently, the average amplitude, shown here as dashed lines, is slightly different for the two ions. The amplitudes and frequencies in this figure are chosen to make the effect visible.

is an appreciable shift $\frac{\Delta\nu_+}{\nu_+} \approx -\frac{k_B T_+}{mc^2} \approx -0.1\,\text{ppt}$ (for medium heavy highly charged ions cooled via the axial resonator including feedback) of the cyclotron frequencies[4]. Since the cyclotron motion is excited for the phase sensitive measurement (either PnA or PnP), the shift during the relevant evolution time can be much larger. For a reasonably good phase resolution the cyclotron motion is excited to an energy of typically $10\,k_B T_+$ leading to an average shift in the order of 1 ppt, or about 10 ppt for light ions. For good mass doublets this shift cancels mostly if both ions are excited to the same radius. However, this requires the spectral transfer function for the respective excitation line to be constant in the respective range of frequencies, which is not necessarily the case especially if the two ions have significantly different cyclotron frequencies. Luckily, to some extent this mismatch of cyclotron amplitudes can be calibrated utilizing an engineered electrostatic (an-)harmonicity. Further imperfections originate from the presence of two ions in the trap. As the masses of two dissimilar ions are not identical, the coupled ions trajectory is never exactly a pure circular "separation" motion around the trap center and the average radius of the two ions becomes slightly dissimilar, depending on their mass difference (see figure 3.6). In combination with unavoidable residual field imperfections this leads to small shifts of the CFR, which scales strongly with d_{sep}^5. On the other hand, for small d_{sep}, the Coulomb interaction between the ions becomes large and shifts all trap frequencies. Interestingly, if the mass difference is very small, the Coulomb interaction causes a resonant interaction of the cyclotron motions and a correspondingly large frequency pushing effect. Consequently, the ion balance method is mostly useful for measurements on good - but not too good - mass doublets. For measurements on the spin precession the choice of ions is larger because the almost electrostatic Coulomb interaction of the ions does not

[4]Note that for the spin precession frequency the corresponding shift is drastically reduced by a factor about $\frac{\nu_+}{\nu_L}$

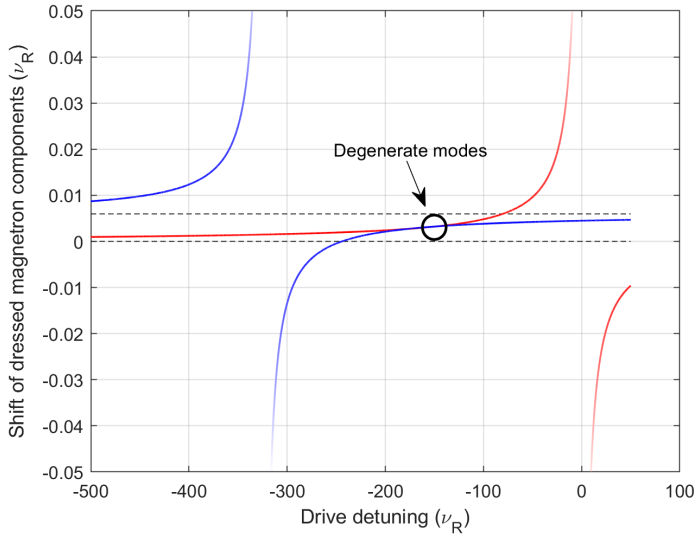

Figure 3.7: Dressing of the magnetron motion with an off-resonant Q_{xz} drive close to the $\nu_z + \nu_-$ sidebands. For a suitable coupling strength the magnetron frequencies of two dissimilar ions can be made exactly degenerate by choosing a coupling frequency right in between the unperturbed sidebands. This way, the ions scan the same radius and systematic shifts due to trap imperfections are significantly reduced.

strongly influence the spin precession so that d_{sep} can be chosen much smaller. Finally, it is conceivable to add a q/m dependent force in order to null the magnetron frequency difference of the two ions. Such a force can be for example an off-resonant axial-magnetron Q_{xz} coupling drive as suggested already in [49], or a Q_{zz} drive above the axial frequency. In the first case the magnetron motion of both ions is dressed by the respective axial motion, but since the axial frequencies are slightly different the detuning is also different for both ions and the resulting magnetron frequency shifts can be chosen to make the absolute magnetron frequencies degenerate (see fig. 3.7). If the drive is sufficiently far detuned, the change in the separation radius due to the axial-magnetron coupling can be negligible on the time-scale of a single measurement shot. In the latter case, an extra effective potential, similar to a radiofrequency ("Paul") trap, which depends on q/m is added to the static trap and can be tuned to null the magnetron frequency difference. In both cases the systematic shifts associated with the slightly imperfect matching of the trajectories can be significantly reduced and a correspondingly higher precision can be achieved.

4 | Zeeman spectroscopy

The strong magnetic field in the Penning trap not only makes the ion rotate with the cyclotron frequency, but also causes a Zeeman splitting due to the alignment of the (internal) magnetic moment $\vec{\mu}$ of the ion relative to the magnetic field. For an s-state atomic ion without nuclear spin, $\vec{\mu}$ is proportional to the spin vector $\vec{S}$

$$\vec{\mu} = -g_S \mu_B \frac{\vec{S}}{\hbar}. \tag{4.1}$$

The unitless "g-factor" is typically $g_S \approx 2$. The exact value of g_S can be calculated from first principles using QED to extraordinary precision for many systems and is thus subject of active research. A comparison of the calculated g to a measured value can thus, especially in HCI, be used to test the theory. My group has contributed a number of measurements to this field, among others:

- **Most stringent test of QED in strong fields:**

  S. Sturm et al. "g factor of hydrogenlike $^{28}Si^{13+}$". In: *Phys. Rev. Lett.* 107.2 (2011), p. 023002

- **Most stringent tests of relativistic many-electron calculations in strong fields:**

  A. Wagner et al. "g factor of lithiumlike silicon $^{28}Si^{11+}$". In: *Phys. Rev. Lett.* 110.3 (2013), p. 033003,

  D. Glazov et al. "g Factor of Lithiumlike Silicon: New Challenge to Bound-State QED". in: *Phys. Rev. Lett.* 123.17 (2019), p. 173001

  and

  I. Arapoglou et al. "g Factor of Boronlike Argon $^{40}Ar^{13+}$". In: *Phys. Rev. Lett.* 122.25 (2019), p. 253001

- **The isotopic shift in highly charged calcium:**

  F. Köhler et al. "Isotope dependence of the Zeeman effect in lithium-like calcium". In: *Nat. Commun.* 7.1 (2016), pp. 1–8

- **The electron mass in atomic mass units:**

  S. Sturm et al. "High-precision measurement of the atomic mass of the electron". In: *Nature* 506.7489 (2014), pp. 467–470

  F. Köhler et al. "The electron mass from g-factor measurements on hydrogen-like carbon $^{12}C^{5+}$". In: *J. Phys. B-At. Mol. Opt.* 48.14 (2015), p. 144032.

This chapter gives a brief introduction to the basics of these measurements and introduces our measurement campaigns. Much more detailed information can be found in our original publications.

For any state with non-zero orbital angular momentum ($l > 0$) the expression for the magnetic moment becomes slightly more complex as the g-factor of the orbital angular momentum $g_L = 1$ is significantly different from $g_S \approx 2$, so that $\vec{\mu_J} = g_L\vec{L} + g_S\vec{S}$ is not co-linear with the total angular momentum vector $\vec{J} = \vec{L} + \vec{S}$. Still, the absolute value μ_J can be written in units of the total angular momentum norm and the Landé g-factor g_J:

$$|\vec{\mu_J}| = g_J\mu_B\frac{|\vec{J}|}{\hbar}. \tag{4.2}$$

In a Penning trap the projection of the magnetic moment on the magnetic field can take discrete values:

$$\mu_{J,z} = g_J\mu_B m_J, \tag{4.3}$$

where m_J takes values $m_J \in [-J : 1 : J]$. Each of these orientations has its specific energy in the magnetic field:

$$\Delta E = -\mu_{J,z}B_0. \tag{4.4}$$

Consequently, the orientation of the magnetic moment can be altered by a photon with suitable energy $E_\gamma = 2\Delta E = \hbar\omega_L$. Here, the Larmor frequency ω_L also quantifies the oscillation of μ_J around the magnetic field axis. However, unlike the ion's motion in the trap, the Larmor oscillation cannot directly be detected. Rather, we probe the "spin-flip" resonance[1] with suitable millimeter-wave photons and find the frequencies for which the probability to observe a change of m_J becomes maximal. To this end, we need a method to determine m_J for an arbitrary single ion. In some cases this is possible by observing optical fluorescence photons, if a suitable "shelving" transition is available (see fig. 4.1,[55]) in the ion of interest. For the few-electron, highly charged ions that we are interested in this is generally impossible due to a lack of suitable transitions. Here, we add a strong magnetic bottle to our Penning trap, so that the magnetic moment projection becomes visible via a shift of the axial frequency (CSGE). By injecting millimeter wave photons with about the Larmor frequency, the spin-state can be flipped and consequently the axial

[1] Technically, this term is incorrect, as in $l \neq 0$ ions not necessarily the spin is flipped, but the magnetic moment orientation is changed. I use the term "spin-flip" in this general sense.

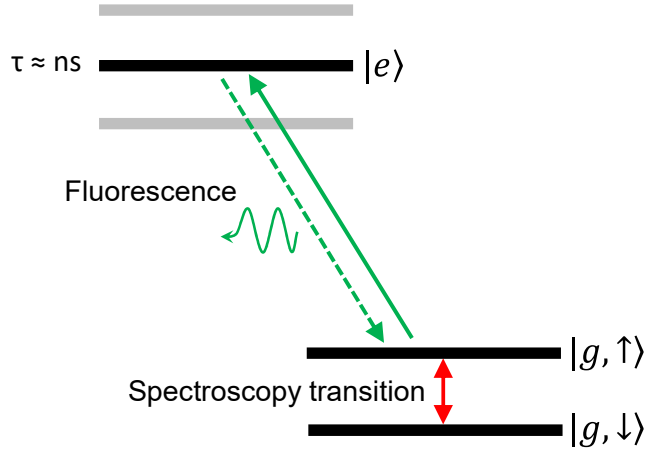

Figure 4.1: Direct electron shelving technique. The optical transition between states $|g,\uparrow\rangle$ and $|e\rangle$ can be strongly driven and the resulting fluorescence photons are detected. Fluorescence ceases when the (millimeter-wave) spectroscopy pulse drives the ion into the dark Zeeman sub-state $|g,\downarrow\rangle$. In many cases however, especially in few-electron HCI, no suitable state $|e\rangle$ is available for detection.

frequency changes measurably. In principle, by measuring the cyclotron frequency (eq. 2.1) of the ion in the same magnetic field, the magnetic moment of the ion can be determined from the ratio Γ of ω_L and ω_c in units of the ion mass and charge:

$$\Gamma = \frac{\omega_L}{\omega_c} = 2\frac{m_{\text{ion}}}{q_{\text{ion}}}\mu_{J,z} = g_J\frac{m_{\text{ion}}}{q_{\text{ion}}}\mu_B = \frac{g_J}{2}\frac{e}{q_{\text{ion}}}\frac{m_{\text{ion}}}{m_e}. \tag{4.5}$$

If the ratio of electron to ion mass is known from other experiments, we can express the g-factor as:

$$g_J = 2\Gamma\,\frac{q_{\text{ion}}}{e}\frac{m_e}{m_{\text{ion}}}. \tag{4.6}$$

In the strong magnetic bottle of the ALPHATRAP "analysis trap" (AT) of about $B_2 = 43\,000\,\text{T}\,\text{m}^{-2}$, the finite energy of the axial and cyclotron motions causes large shifts of all frequencies and consequently the measurement precision is limited. A simple estimate of the resonance width can be obtained by considering the thermal axial amplitude (eq. 3.2). As the axial amplitude changes on a millisecond time-scale when the ion is in thermal equilibrium with the tank circuit, the Larmor resonance is broadened to

$$\frac{\delta\omega_L}{\omega_L} = \frac{B_2}{2B_0}\hat{z}_{\text{th}}^2 \approx 10^{-6}. \tag{4.7}$$

A drastic improvement can be achieved with the dual-trap technique. To this end, we use a second spatially separated trap, the "precision trap" (PT). Here, the magnetic field is very homogeneous, and consequently the resonances are drastically (typically four orders of magnitude) more narrow compared to the AT. The measurement sequence is then based on the (valid) assumption that the spin state is unchanged when the ion is transported between the two traps. First, we determine the spin state in the AT by observing the axial frequency jump following a spin flip induced by a high-power excitation[2]. Then, after

[2]It is typically insufficient to only measure the axial frequency as the cyclotron energy and voltage source instability can lead to fluctuations comparable to the spin flip.

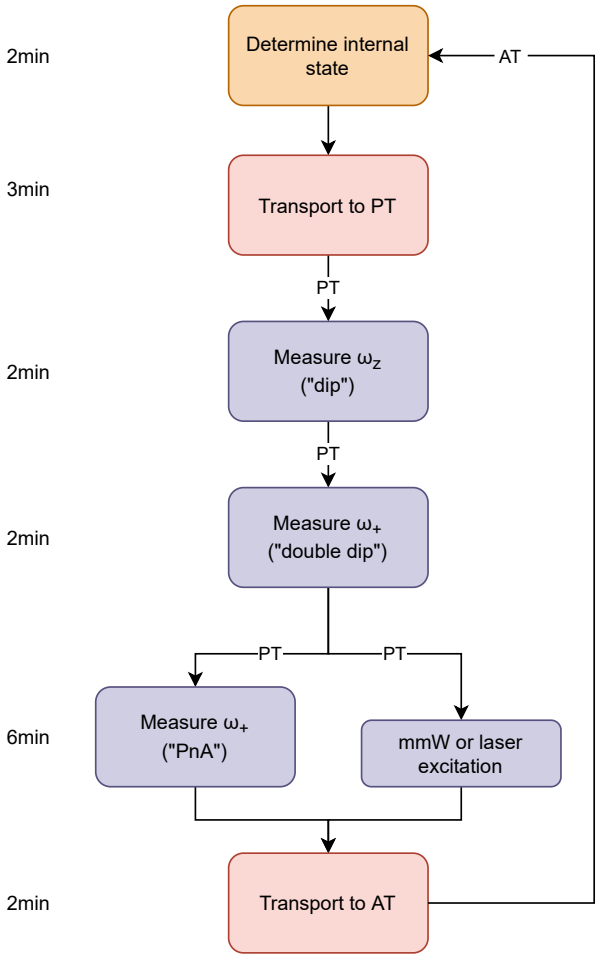

Figure 4.2: Typical measurement sequence for internal state spectroscopy using the CSGE and a dual-trap setup. After we determined the internal state in the AT, we transport the ion to the PT, where we measure the cyclotron frequency with PnA and simultaneously inject a probe pulse (laser or mmW). Finally, the resulting internal state is determined again in the AT. The approximate times noted at the side include wait periods to let voltages settle. The truly sensitive spectroscopy time is only about 5-10s at the end of the PnA sequence. One such cycle takes less than 20 minutes.

transporting to the PT, we measure the cyclotron frequency and simultaneously introduce a millimeter-wave excitation at a random frequency. If this frequency is close enough to the true Larmor frequency in that specific magnetic field, the spin can be flipped. The result is tested after transporting back to the AT. One such cycle gives us a value of

$$\Gamma'_i \equiv \left(\frac{\omega_{\mathrm{mw}}}{\omega'_c}\right)_i \tag{4.8}$$

and the Boolean information S_i whether the spin flipped or not. This tuple $T_i \equiv (\Gamma'_i, S_i)$ is self-consistent and basically independent of time and magnetic field, as fluctuations of B_0 between cycles drops out. We will see later that this is not true for fluctuations of B_0 within the excitation time. The set of T_i resulting from many such cycles can then be combined to plot the fractional spin-flip rate as a function of the unitless ratio Γ. A histogram of the fraction of "sucessful" T_i reveals a narrow resonance from which the magnetic moment can be determined. To avoid artifacts from the binning process, we use a maximum-likelihood fit to the original unbinned T_i to determine the resonance center. In the ALPHATRAP PT, errors from field imperfections are negligible. The resonance width originates from a combination of the finite measurement precision of the cyclotron frequency (with the

phase-sensitive PnA method) and magnetic field fluctuations within the measurement time. For HCI, PnA achieves typically about 6-10° phase precision. For a 5 second spectroscopy pulse this translates (compare eq. 2.15) into $\frac{\delta\nu_c}{\nu_c} = \frac{10°}{360°\,5\,\mathrm{s}\,28\,\mathrm{MHz}} \approx 2 \times 10^{-10}$ relative precision. Additionally, as PnA measures the mean magnetic field $\langle B_0(t)\rangle_t$ during the evolution time, the microwave drive is incoherent with respect to the Larmor precession (as in a Rabi-type experiment) on the timescale of 5 seconds. Consequently, magnetic field fluctuations in a frequency range from 0.2 Hz up to about 100 Hz contribute to the resonance width. Here, the upper limit is connected to the modulation index [56] of the Larmor precession $\eta(\omega) \equiv \frac{\Delta\omega_L}{\omega} = \frac{\Delta B_0(\omega)}{B_0}\frac{\langle\omega_L\rangle}{\omega}$, which is significantly larger than for the cyclotron motion. Consequently, for magnetic field fluctuations no larger than 1 ppb the resonance will show significant contributions for $\eta \gtrsim 1$, or $\omega \lesssim 2\pi\,100\,\mathrm{Hz}$, which is also empirically confirmed. It is thus of prime importance to reduce the amount of field fluctuations in this "acoustic" range. Interestingly, the eddy current decay time in the closed cryogenic trap chamber, manufactured from OFHC copper, is expected (not measured) to be around $\tau \approx 100\,\mathrm{ms}$ and consequently external fluctuations $\gg 1\,\mathrm{Hz}$ should be efficiently suppressed. Future upgrades should therefore not only improve the shielding factor, for example by implementing a superconducting magnetic shield around the trap chamber, but also improve the internal mechanical stability of the trap setup. This is because any change of the geometry, originating either from external vibrations or changes of the local temperature, generate field fluctuations for the ion that are not shielded by external measures. At the current state, typically a (relative) resonance FWHM of about 1 ppb is achieved. With sufficient statistics and for a non-saturated resonance the line center can then be determined to a few 10 ppt. This experimental precision surpasses, with the exception of the lightest ions, the current state-of-the-art theoretical predictions and consequently allows testing even high order contributions of QED in the strong fields that are found in HCI.

4.1 Testing quantum electrodynamics in the strong field regime

Highly charged ions are extraordinarily good systems for probing the boundaries of validity of our fundamental theories. This is owing to a combination of two unique properties:

- Even heavy HCI can have only single or few electrons, such that they are very accessible for precise and rigorous calculations from first principles.
- The electrons are located very close to the nucleus, where they experience the strongest fields we have available in the laboratory in stable systems. These can

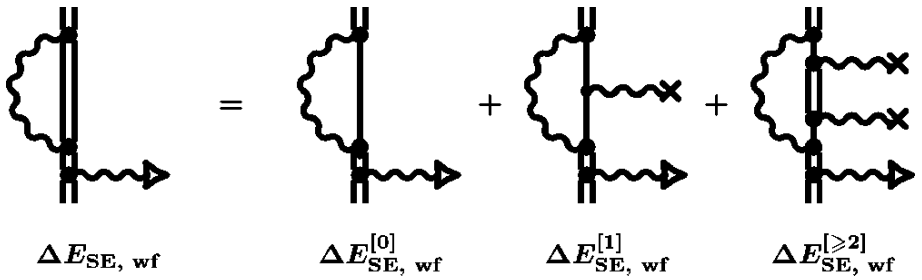

Figure 4.3: Example for the $(Z\alpha)$ decomposition of a bound-electron Feynman diagram, in this case the self-energy contribution. The double line stands for a bound-state electron propagator, whereas single lines are the more simple free electron version. The effect of the Coulomb binding, which is rigorously included in the bound-electron propagator, is expanded here in individual photon exchange vertices, with photon lines that end in a cross. The coupling at these vertices depends on $Z\alpha$, so that an increasing amount of such vertices is required to reach sufficient precision in high-Z ions. Figure taken from [57].

reach beyond 10^{16} V cm^{-1} for the electric and 20 000 T for the magnetic fields (for ions with nuclear spin).

Over the years, leading theory groups have calculated many contributions to g. Depending on the Z regime, two different methods for dealing with the binding of the electron to the nucleus are used. For low-Z ions, two expansions are used, one for the loops of the interaction with the vacuum, proportional to α^n, and a second one in orders of $(Z\alpha)^n$ that describes the interaction with the binding field. This effectively corresponds to assuming the electron does interact with the nucleus only via virtual photons and evolves freely in between interactions. This simplifies the calculation, as the plane wave propagator is used in the calculation of the Feynman diagrams. This method has been pioneered by Prof. Krzysztof Pachucki and is called (non-relativistic) NR-QED. For small Z this second series converges quickly and provides very good precision. For large Z however, $Z\alpha$ approaches unity and is thus no good expansion parameter anymore (see figure 4.4). Now, bound-state QED becomes a strongly coupled theory and we have to give up the assumption of a free electron in between interactions but use the known hydrogen solution for the propagator. While this takes care of the strong interaction with the nucleus (in all orders of $Z\alpha$), it makes the calculation significantly more involved. Then again, this regime of QED has never been tested to high precision before and is consequently highly interesting for experiments. Another way to look at that is apparent in figure 4.4, where the higher-order in $Z\alpha$ contributions become dominant for high Z.

Over the last years my group has worked towards performing the most stringent tests of QED in strong fields and towards reaching the highest Z regime. This series of experiments has initially been started at the Johannes Gutenberg University in Mainz in the group of Prof. Dr. Günter Werth in collaboration with Dr. Wolfgang Quint and Prof. Dr.

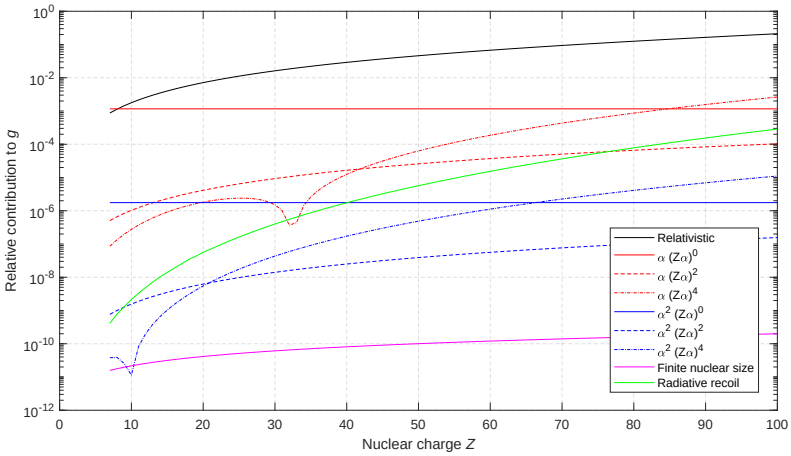

Figure 4.4: Non-exhaustive compilation of (relative) contributions to the bound-electron g-factor in hydrogenlike ions. It is clearly visible how the higher-order in $(Z\alpha)$ contributions become dominant for high Z and eventually even surpass the leading order $(Z\alpha)^0$ contribution [58].

Heinz-Jürgen Kluge, and has later been continued in the group of Prof. Dr. Klaus Blaum, where I pursued my PhD thesis. There, in the apparatus that now has been reconstructed to LIONTRAP, the g-factors of hydrogenlike carbon [59] and later oxygen [60] have been measured and successfully compared to theory. However, this experiment is hermetically sealed with a pinch-off tube and so ions have to be produced in-situ, which was limited in this setup to low-Z ions.

4.1.1 The most stringent test of QED in strong fields

In the course of my PhD thesis we have upgraded this setup to allow both for higher electron beam energy and also precision. This way, using the then newly developed PnA method we were able to measure the g-factor of hydrogenlike silicon $^{28}Si^{13+}$ [50, 33] with 11 digits precision and compare it with QED theory. The limitation of this test is currently the uncertainty due to the uncalculated higher order terms, at the time of our measurement $\alpha^2\,(Z\alpha)^{5+}$. Since then, also most $\alpha^2\,(Z\alpha)^5$ terms have been calculated so that today the precision of the comparison has increased to 3×10^{-10}, testing not only electron QED contributions up to 3-loop level and specific bound electron contributions up to 2-loop level, but also contributions by the nuclear size as well as the relativistic recoil. The agreement of experiment and theory thus constitutes the most stringent test of QED in strong fields.

4.1.2 The deviation in lithiumlike HCI

But the measurement principle is not limited to single electron systems. By adding two electrons, the 1s shell is filled and one unpaired spin remains in the 2s shell. This lithiumlike configuration experimentally behaves very much alike the hydrogenlike one, however on the theory side the calculation has to include the effect of the inner shell electrons and their fully relativistic interaction with the active 2s electron. Indeed, a

Table 4.1: Contributions to the g-factor of $^{28}Si^{13+}$. Our experiment probes QED contributions up to order $\alpha^2 (Z\alpha)^5$, but also contributions from the nucleus, such as the relativisitic recoil and the charge radius of the nucleus. The dominant uncertainty stems from uncalculated higher orders in $(Z\alpha)^{6+}$. Some of these contributions have been calculated after our results were published, making this test even more stringent than before. The table is based on data from Dr. Zoltán Harman [58].

$\langle r^2 \rangle$ [fm]		3.1223(24)
Dirac value		1.993 023 571 6
Finite nuclear size		0.000 000 020 45
One-loop QED		2 328 682 623(6)
Two-loop QED	$(Z\alpha)^0$	−0.000 003 544 610
	$(Z\alpha)^2$	−0.000 000 006 166
	$(Z\alpha)^4$	−0.000 000 002 255
	$(Z\alpha)^5$	0.000 000 000 284
	$(Z\alpha)^6$	0.000 000 000 000(583)
Three-loop QED	$(Z\alpha)^0$	0.000 000 029 498
	$(Z\alpha)^2$	0.000 000 000 051
Recoil	Non-QED	0.000 000 204 534(1)
	rad-rec	0.000 000 001 600(100)
	Radiative	−0.000 000 000 159
	$(m/M)^2$	−0.000 000 000 060
Total Theory		1.995 348 957 347(592)
Total Experiment		1.995 348 957 663(111)

measurement [51] in my group has probed this and found agreement within the theory uncertainty, justifying our understanding of relativistic dynamics in strong fields. However, later we have revisited this system with significantly higher precision both experimentally as well as on the theory side [52] and found a 1.7σ tension. A further improvement of the theory [61] confirms the previous finding, however it is more precise and thus enlarges the discrepancy to over 3 standard deviations. A second measurement of our group on lithiumlike calcium isotopes (see section 4.3) reveals an even larger 4.5σ deviation. These discrepancies are still standing today and a challenge for QED theory, as it is believed [58] that a significant contribution is missing.

4.1.3 Towards the $Z\alpha \approx 1$ regime with ALPHATRAP

Ultimately, the goal of my group is to perform a precise test of QED in the $Z\alpha \approx 1$ regime, around hydrogenlike lead $^{208}Pb^{81+}$. To this end, two important requirements need to be fulfilled:

- In the ion source an ionisation energy of 105 keV has to be overcome. For an electron beam ion trap (EBIT) this means reaching a beam energy in excess of 200 keV.
- The vacuum in the trap needs to be better than 10^{-17} mbar to allow storing the ion, which has a large tendency to pull electrons from rest-gas atoms and molecules, for at least a few days.

While the second requirement has been fulfilled already at least in the hermetically sealed, cryogenic traps such as LIONTRAP, the first one is technically impossible in an in-situ

EBIT inside the trap chamber. Rather, big and specialised facilities have to be used. These can be grouped into ion beam and electron beam based sources. At the ESR storage ring at GSI Helmholtzzentrum für Schwerionenforschung in Darmstadt lowly charged ions impinge with high energy, typically about 400 MeV per nucleon, on a stationary stripper foil. This energy of the ions is high enough so that the kinetic energy of the bound electrons overcomes their ionisation energy. After the stripper a large number of HCI up to the highest charge states results, however, their kinetic energy spread is large. These ions need to be cooled by many orders of magnitude before they can be captured in a precision trap. This challenging endeavor is currently pursued at the HITRAP facility at GSI.

At MPIK we instead use the HD-EBIT, a facility developed and run by José Crespo, which uses a high energy electron beam impinging on stationary ions. In that case, the electrons needs much less energy than the ions in the above case, ideally about 2-3 times the ionisation energy, about 200 keV to 300 keV for hydrogenlike lead. Currently, this is beyond the capabilities of the HD-EBIT, but in a collaboration between my group within the division of Klaus Blaum and the group of José Crespo, a major upgrade project is on its way that aims to reach these energies (see chapter 6). With the current HD-EBIT we can reach up to 70 keV beam energy, sufficient to produce hydrogenlike tin $^{118}Sn^{49+}$.

In order to inject these ions into the cryogenic precision trap, we have to connect the trap chamber to a room-temperature beamline. ALPHATRAP has been constructed specifically to allow the injection from external ion sources, without compromising the in-trap vacuum. To this end, we have developed the, to our knowledge, first cryogenically operable XHV vacuum valve. This valve is opened for the injection and closed afterwards, leaving the trap vacuum completely sealed. It is now imperative that the amount of rest-gas, specifically hydrogen, that enters the trap during this time is limited. As long as the total accumulated amount of gas is less than the equivalent of a few monolayers on the surfaces of the trap chamber, the hydrogen (and also helium) relatively strongly sticks to the cold walls despite its relatively sizeable vapour pressure at 4 K. Recently, we have demonstrated the uninterrupted storage of hydrogenlike $^{118}Sn^{49+}$ for more than 2 months before it recombined to $^{118}Sn^{47+}$, compatible with a rest-gas pressure of about 10^{-17} mbar. This is sufficient for extended trap measurements on even the highest charge states or antimatter particles. Today, ALPHATRAP is performing measurements on the highest charge states of ^{118}Sn, where $Z\alpha \approx 0.36$, which will be a big step towards the highest field strengths and open a unique view into unknown terrain of strong field QED.

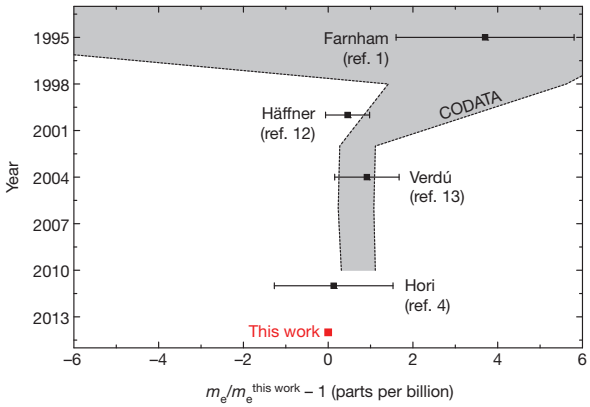

Figure 4.5: Determinations of the electron atomic mass until 2014. Our value, denoted here as "this work", is more than a factor of 13 more precise than previous values averaged from measurements on antiprotonic helium (Hori [62]), bound-state electrons g-factor (Verdu[60] & Häffner[59]) and cyclotron frequency ratios (Farnham[63]). The recent HD^+ results are missing in this plot, which was taken from [37].

4.2 The electron mass from the bound electron g-factor

The excellent agreement for hydrogenlike systems motivates an alternative use of the g-factor experiment: If we trust in the validity of QED theory, we can take the left side of equation 4.6 as given. Then, by measuring Γ, we can determine the ratio of electron and ion mass (assuming that the charge ratio is a known integer). In principle the choice of the ion is arbitrary, but it is especially useful to take $^{12}C^{5+}$. Carbon is the basis of our atomic mass unit u and so the atomic mass of hydrogenlike carbon is known to extraordinary precision, limited only by the uncertainty of the binding energy of the 5 missing electrons. Using all newly developed methods and the new trap, in 2014 we have published our value of the electron mass with 28 ppt precision, over an order of magnitude more precise than the previously tabulated value in the CODATA compilation of fundamental constants and about 1.5σ lighter (see figure 4.5). Today, our value is influencing a wide range of fundamental atomic physics, among others the interpretation of the spectrum of the hydrogen atom [19] and the HD^+ molecular ion [20, 21] and the determination of the finestructure constant α in photon recoil measurements. Only recently, ultra precise measurements of ro-vibrational transitions in the HD^+ molecule have become competitive with this value. Combined with an independent determination of the proton-to-deuteron mass ratio and our determination of the proton and deuteron atomic masses, these allow comparison with our electron atomic mass value. Fascinatingly, the values agree, a truly beautiful confirmation of our understanding of atomic physics. Here, direct cyclotron frequency measurements, bound-state QED in highly charged ions and QED in molecules are combined and agree on a 11 digits level. In the future, a further improvement of the electron mass determination with HCI is anticipated at ALPHATRAP. As magnetic field fluctuations are the limiting factor for the achievable precision, a significant improvement would strongly benefit from a field stabilisation.

4.3 Larmor frequency difference measurements

The comparison of the calculated bound electron g-factor with experiment is currently for most systems limited by theory precision. The uncertainty can originate from uncalculated higher-order QED contributions, but also from parameters that enter the calculation. For spin-less nuclei these parameters are mostly the nuclear charge radius, nuclear mass and other nuclear properties and the finestructure constant α, all of which are known from other experiments, but with limited precision. In many cases, these uncertainties can render other small but interesting contributions invisible. An effective way to make these small effects visible is to investigate the difference of two g-factors in similar systems, where many common contributions drop out. Suitable candidates for such difference measurements are either different charge states of the same nucleus or different isotopes of the same element and charge state.

In the first case, it is for example possible to zero the contributions of the nucleus to a specific difference of g-factors of, for example, hydrogen- and lithiumlike ions $\Delta g = g_{2s,Z} - \Xi_Z g_{1s,Z}$. Here, typically $\Xi_Z < 1$ because the nuclear properties influence the 1s state much more than the 2s. The precise value of Ξ_Z has been calculated in [64]. A measurement of Δg can then be used to determine the value of other input parameters, such as the finestructure constant α.

Alternatively, the difference of $\Delta g = g(Z, N_1) - g(Z, N_2)$ for two isotopes (with neutron numbers N_1 and N_2) of the same element allows dropping most QED contributions of the electrons, keeping only those that explicitly depend on the nucleus. Dominantly, these are the finite nuclear size and the finite nuclear mass, which leads to a purely relativistic recoil term. In 2016, my group measured $\Delta g_{\mathrm{Ca}} = g(20, 20) - g(20, 28)$, the isotopic difference between $^{48}\mathrm{Ca}^{17+}$ and $^{40}\mathrm{Ca}^{17+}$ [53]. As we measured these two g-factors individually, we needed the atomic masses of the two HCI to determine g from the measured frequency ratios Γ. To this end, we collaborated with the SHIPTRAP group at GSI Darmstadt, who measured the atomic mass of $^{48}\mathrm{Ca}^{17+}$. The resulting precision for Δg_{Ca} allowed resolving the nuclear recoil effect to about 10% for the first time. The result was limited by the uncertainty of the atomic mass measurement of effectively about 0.6 ppb, while the frequency ratio and the theoretical prediction is more precise. Since the recoil effect is purely relativistic, it requires calculations beyond the Furry picture and the agreement of experiment and theory manifests the validity of our understanding of this type of physics.

4.3.1 Coupled magnetron orbit Zeeman spectroscopy

However, to observe the interesting QED contribution to the recoil a relative precision far in excess of 50 ppt would be required for Δg_{Ca}. To this end the two major limitations have to be overcome, the atomic mass precision and the magnetic field fluctuations that limit Γ.

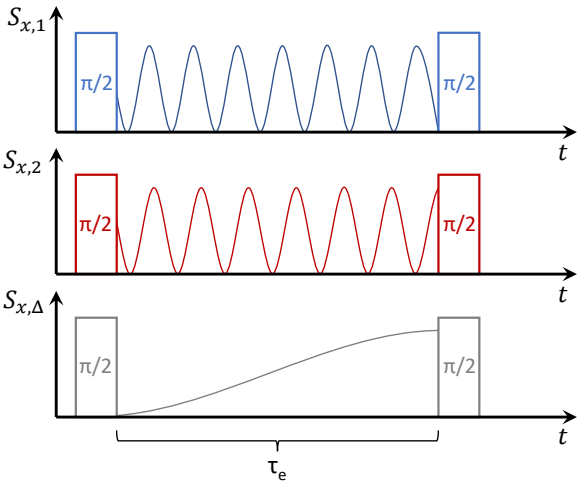

Figure 4.6: Simultaneous dual-Ramsey cycle. Initially, the spins of both ions are brought to the equator of the Bloch sphere with a $\pi/2$-pulse (or two separate pulses) (top and middle). The diagrams indicate the x projection of the spin vector. After some time the spins have evolved and their phases become unpredictable due to magnetic fluctuations. However, the difference of the two vectors (bottom), rotating at a much lower frequency, stays coherent and contains the information of the g-factor difference. At the end of the sequence, a second $\pi/2$-pulse projects both spin onto the magnetic field axis.

An elegant solution to this is to measure the Larmor precession of two ions simultaneously in coupled magnetron orbits, similar to the method described in 3.4.1. In that case, the ions are almost exactly at the same position on average, and exchange position every magnetron half-cycle, roughly every 50 µs (compare fig. 3.5). This rapid swapping of the ions strongly suppresses not only fluctuations of the homogeneous magnetic field, but also inhomogeneous components on a time-scale longer than $\tau_{\text{crit}} = 1/\nu_-$.

For different isotopes of the same element, but also for different elements with similar Z, the Larmor frequencies are extremely similar, in the case of calcium $\Delta g_{\text{Ca}} \approx 1 \times 10^{-9}$. Consequently, all common magnetic field fluctuations are strongly suppressed in the difference. Moreover, since both ions are located in the same magnetic field at the same time, only a single measurement of B is required. That measurement again, and consequently the atomic mass, is required only to a precision that is reduced by $\Delta g/g \lesssim 1 \times 10^{-7}$ (for isotopes). However, since $\nu_L \gg \nu_c$, any fast fluctuations ($\tau < \tau_{\text{crit}}$) of B will have a much larger effect on the Larmor phase $\varphi_L(\tau) = \omega_L \tau$. If the total accumulated phase difference $\Delta\varphi_L \equiv \varphi_{L,1}(\tau) - \varphi_{L,2}(\tau)$ is predictable to better than 2π, the difference of the Larmor frequencies can be measured coherently. To this end, a simultaneous time-Ramsey cycle is performed (see fig. 4.6). Starting w.l.o.g. from the state $|\downarrow\rangle\,|\downarrow\rangle$, for two resonant $\pi/2$-pulses the probability to find the spin of ion 1 in state $|\uparrow\rangle$ is given by:

$$p_{1,\uparrow}(t) = \sin^2\left(\omega_{L,1} t + \varphi_{1,0}\right). \tag{4.9}$$

Consequently, the probability to find either $|\downarrow\rangle\,|\downarrow\rangle$ or $|\uparrow\rangle\,|\uparrow\rangle$ can be written as a product:

$$p_{\parallel}(t) = p_{1,\uparrow}(t)p_{2,\uparrow}(t) + p_{1,\downarrow}(t)p_{2,\downarrow}(t) = \frac{1}{2} + \frac{1}{4}\cos\left(2\left(\Delta_{12} t + \Delta\varphi_{12,0}\right)\right) + \ldots, \tag{4.10}$$

where $\Delta_{12} \equiv \omega_{L,1} - \omega_{L,2}$ is the sought-after difference of Larmor frequencies. In the last

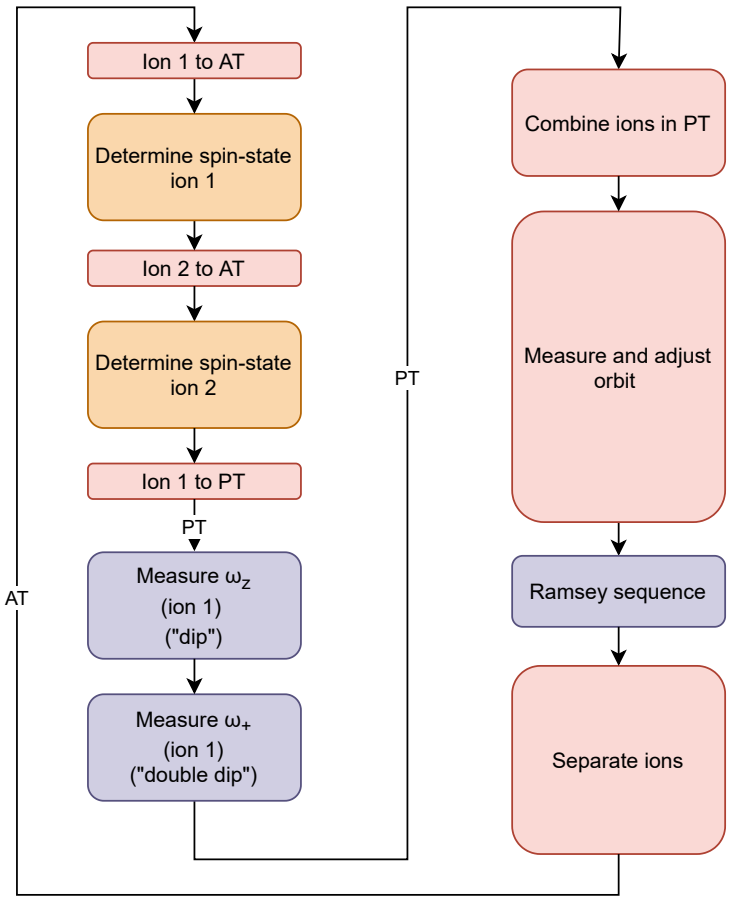

Figure 4.7: Simplified measurement sequence for the simultaneous coherent g-factor difference method. First, the spin-state of both ions, one at a time, is determined in the AT. Afterwards, one ion is transported to the PT, where it is used (as single ion) to measure the cyclotron frequency. Afterwards, the two ions are combined and prepared in a suitable coupled orbit. There, the dual-Ramsey excitation sequence is executed, the ions are separated with the help of the magnetic bottle and the next cycle starts. One such cycle takes about 50 minutes. The size of the blocks roughly indicate the time required for the steps.

step, terms with the original Larmor frequencies and their sum have been neglected. This is generally valid for longer times t, because they quickly become incoherent and then average to zero between measurements. Thus, the correlation of the Larmor oscillations can be mapped onto the spin-flip probability $p_{\parallel}$ (or the equivalent combination $p_{\perp} = p_{1,\downarrow}p_{2,\uparrow} + p_{1,\uparrow}p_{2,\downarrow} = 1 - p_{\parallel}$). The individual probabilities $p_{1,\uparrow,\downarrow}$ and $p_{2,\uparrow,\downarrow}$ can be determined by separating the ions and detecting their spin-state, one at a time, in the AT. The complete cycle is depicted in figure 4.7.

Compared to the coupled magnetron orbit method for CFR, here, the frequency shifts due to the Coulomb interaction play a much smaller and simpler role. The Larmor frequencies themselves are almost independent of the electric field for the small velocities at play here, the dominant shifts originate from the slightly imperfect matching of the time-averaged orbits. For two non-identical ions, the average magnetron radius is not perfectly identical (compare chapter 3.4 and figure 3.6). In combination with unavoidable residual magnetic field imperfections this leads to a systematic shift of the Larmor oscillations. A similar shift originates from the dissimilar axial amplitudes when both ions are cooled by the same tank circuit, one at a time. To bring the second ion in resonance, the axial potential is altered adiabatically (on a timescale that is long compared to the axial frequency), so that the axial amplitudes on average relate as $\left(\frac{\hat{z_1}}{\hat{z_2}}\right)^2 = \sqrt{\frac{q_2 m_2}{q_1 m_1}}$. The axial

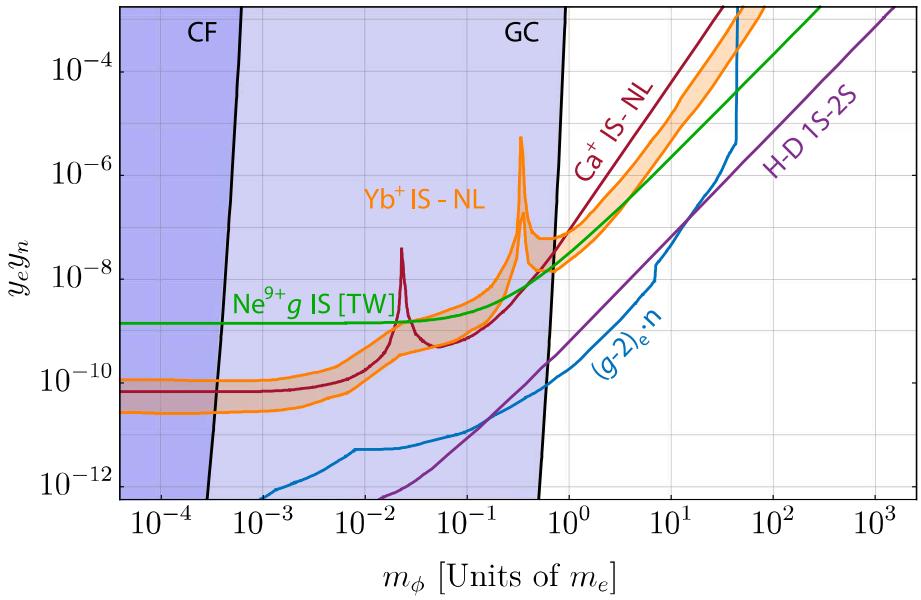

Figure 4.8: Limits for hypothetical bosons of mass m_ϕ and coupling $y_e y_n$ to electrons and nucleons from several experiments. Our Δg measurement can set stringent limits (TW) specifically for the large mass range due the simple electron structure with only a single bound electron close to the nucleus. Other limits shown here include the free electron $g-2$, combined with neutron scattering data [65], measurements of the Casimir force (CF) [66] and astrophysical limits from globular clusters (GC) [67]. The currently most sensitive limit comes from the measurements of the isotope shift in atomic hydrogen (H-D 1s-2s) [68].

amplitudes then cause Larmor frequency shifts from two dominant sources:

- directly, via the motion in the residual magnetic bottle: $\Delta\nu_L \sim B_2\hat{z}^2/2$
- indirectly, via the shift of the axial equilibrium position due to a residual electrostatic asymmetry C_3 and the magnetic gradient B_1: $\Delta\nu_L \sim B_1 C_3 \hat{z}^2$

With current methods, the combined relative shifts due to the magnetron and axial amplitudes can be limited to a level of about 1×10^{-13}. Recently, my group has performed the first such measurement on the $^{20,22}Ne^{9+}$ isotopes of neon. There, the theoretical prediction of the isotopic effect is limited by the tabulated nuclear charge radius difference to 5 ppt, whereas the experimental precision is about an order of magnitude better. The comparison of Δg on this level of precision opens up a new regime for probing the validity of QED. Now, the nuclear recoil contribution can be resolved to 3-4 digits and for the first time the QED contribution to the nuclear recoil can be tested to 25%. A better value for the charge radius difference in the future could even improve this comparison by an order of magnitude. The agreement of experiment and theory also sets stringent limits on new, unknown contributions to Δg. For example, dark matter exchange bosons that couple to

the electron and nucleons via the Higgs portal [9] would lead to a shift of Δg depending on their mass and the coupling constants $y_e y_n$. Consequently, our experiment allows setting limits on such dark matter candidates. Figure 4.8 shows the resulting exclusion plot. These results have recently been submitted to Nature.

5 | Laser spectroscopy

The techniques described in chapter 4 were originally intended specifically for g-factor spectroscopy. However, the ability to distinguish internal metastable substates of single ions with close to unity fidelity, combined with the extremely good vacuum and the stable field conditions, make cryogenic Penning traps also a prime tool to perform precision spectroscopy of forbidden optical transitions. This chapter describes the measurement principles at the example of the first proof-of-principle measurement at ALPHATRAP, the measurement of the finestructure transition in boronlike $^{40}Ar^{13+}$ [17].

Today, precision laser spectroscopy of atomic and molecular ions has become one of the most powerful tools for fundamental research. The trapped ion can be cooled to very low temperatures or even to the motional ground-state. In combination with ultra-narrow lasers and frequency combs, a new regime of precision becomes available. For the highest precision, long-lived states and correspondingly narrow transitions have to be used. However, the long lifetime also causes extremely low fluorescence yields and prevents the traditional detection of those fluorescence photons for detecting a transition. In some specific cases, a second, rapid cycling internal transition can be used to detect fluorescence. In this so-called electron shelving technique the transition to a third long-lived state is detected via the sudden absence of fluorescence from the first transition (see also 4.1). Generally however, such a transition is not available in the ion of interest and other, novel techniques have to be used:

- Quantum logic spectroscopy (QLS)
- continuous Stern-Gerlach effect (CSGE)

For QLS, an auxiliary ion (A) with a rapid cycling transition, for example Be^+, is co-trapped with the ion of interest (S). By laser-cooling A, also S can be sympathetically cooled so that eventually the two ions crystallize. This Coulomb crystal can then be further cooled, for example via resolved sideband cooling, to or close to the motional ground state. Due to the close proximity of the two ions in the crystal, typically about 40 µm, their motion is strongly coupled by the Coulomb force. The internal state of S can thus be mapped onto the motional state of the crystal via a red sideband pulse, resonant with one of the shared motional modes. Afterwards, the motional state is mapped to an internal state of A, where it can be detected via optical fluorescence. Until today, QLS has

mainly been used in radiofrequency traps and enables rapid state detection, but requires a second ion to be co-trapped [69].

In my group we have recently developed a novel scheme on basis of the CSGE that enables a new type of laser spectroscopy. This chapter addresses our method and measurements that become possible with it. Detailed information can be found in the original publication:

- **Laser spectroscopy of HCI via the CSGE**

  A. Egl et al. "Application of the Continuous Stern-Gerlach Effect for Laser Spectroscopy of the $^{40}Ar^{13+}$ Fine Structure in a Penning Trap". In: *Phys. Rev. Lett.* 123.12 (2019), p. 123001.

The idea there is to use a laser beam to drive a transition into a state with different magnetic moment projection. Such a transition can then be detected with almost unity fidelity via the CSGE. This way, no fluorescence photons have to be detected, making the technique largely independent of the decay rate and linewidth of the spectroscopy transition. If the lifetime of the excited state is very long, as typically in very narrow clock transitions, the CSGE is used directly on the excited state.

5.1 Fine structure of boronlike $^{40}Ar^{13+}$

Alternatively, the ion can be pumped into a different ground state via a spontaneous decay. The strong magnetic field in a Penning trap lifts the degeneracy of levels with different m_J. This process is depicted in figure 5.1 at the example of the fine-structure transition in boronlike argon $^{40}Ar^{13+}$. There, the ion is prepared in a well-defined Zeeman substate, here w.l.o.g. the spin "up" ($|g, +1/2\rangle$) state. The laser now probes the transition to $|e, -1/2\rangle$. Due to the Zeeman splitting, even a polarized beam is not strictly necessary. When the

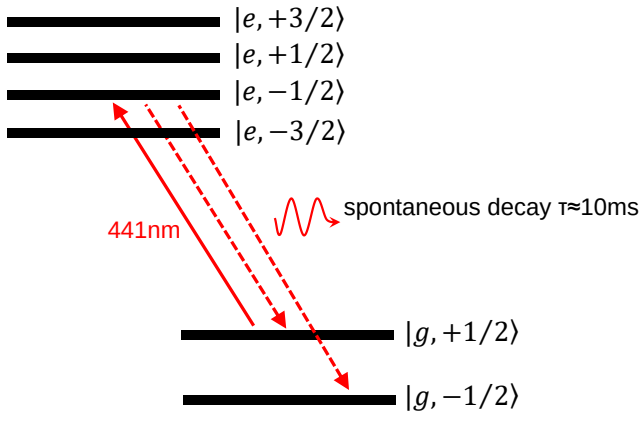

Figure 5.1: Laser spectroscopy of a dipole forbidden transition with long lifetime. The CSGE allows distinguishing between the $|g, \pm 1/2\rangle$ ground states. In this example, initially the ion is prepared in $|g, +1/2\rangle$. If the laser drives the $|g, +1/2\rangle \rightarrow |e, -1/2\rangle$ transition, a spontaneous decay to either $|g, +1/2\rangle$ or $|g, -1/2\rangle$ is possible. Due to the Zeeman splitting, the $|g, -1/2\rangle$ is effectively a dark state that the ion is eventually pumped into. The changed ground state is detected using the CSGE.

ion is excited to $|e,-1/2\rangle$ it can decay back to either $|g,+1/2\rangle$ or $|g,-1/2\rangle$ within roughly 10 ms. In the latter case, the Zeeman shift makes the laser strongly off-resonant, so that the ion is eventually pumped into the $|g,-1/2\rangle$ dark state. The transition can then be witnessed by determining the change of the final state $|g,+1/2\rangle \rightarrow |g,-1/2\rangle$. Since the CSGE can detect this change of state with basically unity fidelity, also extended scans to search for the transition are possible. If the transition lies within the scanned range and the laser power and chirp speed are chosen suitably, the ion will eventually be pumped into the dark state. This can be detected after the scan and a divide-and-conquer algorithm can be employed to narrow in on the transition, so that scan ranges of several GHz are easily possible even for extremely narrow transitions. In our work [17], we have introduced and demonstrated this technique at the example of $^{40}Ar^{13+}$. There, we have achieved a precision of 9 ppb, limited mostly by the calibration of the laser frequency, which was measured by a iodine-locked wavemeter, which had been cross-calibrated with a frequency comb at the start and end of the campaign only. Additionally, the first order Doppler shift at an axial temperature of about 1 K leads to a symmetric broadening of the resonance at f_o to $\sigma_{f_o} = \sqrt{\frac{k_B T_z}{mc^2}} f_o \approx 33$ MHz. In fact, as the ion is strongly trapped, this broadening consists of a "forest" of sideband lines at $\Delta f_o = \pm n_1 f_z \pm n_2 f_- \pm n_3 f_+$. For a plane wave beam, the magnetron and cyclotron sidebands should be weak if the laser is exactly parallel to the magnetic field. The axial sidebands however are sizeable, but could not be resolved in this measurement due to the effective linewidth of the laser. In dedicated experiments the precision can be drastically improved by resolving the individual sidebands, which becomes possible either by cooling to the Lamb-Dicke regime with (sympathetic) laser cooling (see chapter 6.3) or generally by resolving the forest of lines with a laser of suitable stability and linewidth. In either case, the uncertainty due to the first order Doppler shift is zeroed and new limits have to be considered. Depending on the type of transition, these can be the second order Doppler shift (SODS) or magnetic field fluctuations for transitions that show a strong Zeeman shift. For an ion at mK temperature, the SODS amounts to a relative shift on the order of 1×10^{-18}. The magnetic field can be determined to about 11 digits by measuring the cyclotron frequency. Consequently, for a first order Zeeman-shifted line (as in the $^{40}Ar^{13+}$ case), the magnetic field imposes about 1×10^{-15} uncertainty for the optical transition. In many cases however, transitions with drastically reduced magnetic field dependence can be used, removing this limitation.

In the future we want to employ this technique to perform ultra-precision laser spectroscopy of partly extremely long-lived ro-vibrational states in molecular H_2^+ and HD^+ ions, and eventually even the antimatter counterpart $\bar{H}_2^-$, which would be a unique test of the CPT invariance theorem (see chapter 6).

6 | Future projects

In this chapter I present planned projects and prospects for ALPHATRAP and LIONTRAP and the field in general. Some of these are very likely to succeed, for some others the progress in the coming years will decide on the feasibility. However all of them will advance the field and provide new opportunities for intriguing measurements.

6.1 The hyperfine structure of HCI

The measurement of the bound electron g-factor in HCI without nuclear spin enables a test of QED in strong electric fields. However, if the nucleus does have a spin, the electron additionally experiences strong magnetic fields, ranging up to 20 000 T for heavy HCI. These magnetic fields give rise to the hyperfine splitting (HFS) [70], which scales with Z^3 and eventually reaches the optical regime:

$$\Delta E_{\mathrm{HFS}} = \alpha g_I \frac{m_e}{m_p} \frac{F(F+1) - I(I+1) - j(j+1)}{2j(j+1)} m_e c^2 \frac{(Z\alpha)^3}{n^3(2l+1)} F_{\mathrm{HFS}}(N, Z, Q). \quad (6.1)$$

The HFS is proportional to the nuclear g-factor g_I and depends on the orbital, spin-orbital, nuclear and total angular momenta l,j,I and F, respectively. Furthermore, it scales with the main quantum number n^{-3} and the correction factor F_{HFS}, which contains the Bohr-Weisskopf effect (BWE) as well as QED contributions. By measuring the HFS it is thus possible to probe QED also in strong magnetic fields, if g_I and F_{HFS} are known sufficiently well. This is however difficult to fulfill with ab-initio calculations, especially for the BWE. Rather, similar to the case of the bound electron g-factor, a specific difference of the hyperfine energy splitting in different charge states $\Delta E' = \Delta E_{2s} - \xi \Delta E_{1s}$ can be formed, which zeroes the largest part of this nuclear structure contribution. For experimental reasons, we prefer systems where both the hydrogen- and lithiumlike HFS fall into the optical (or laser-accessible) regime. The n^{-3} scaling (see eq. 6.1) means that the hydrogenlike HFS needs to be in the near-UV range, so that we can find the lithiumlike HFS in the IR. This is uniquely possible in the $Z \approx 83$ range, around bismuth $^{209}\mathrm{Bi}^{82+,80+}$.

In 2016, the LIBELLE collaboration has published [71] their results on the bismuth HFS measured at the experimental storage ring ESR at GSI Darmstadt. They reached a relative experimental accuracy of about 3.5×10^{-4} for $\Delta E'$. The comparison with theory, using the tabulated value of the nuclear g_I-factor (obtained via liquid-phase NMR), showed

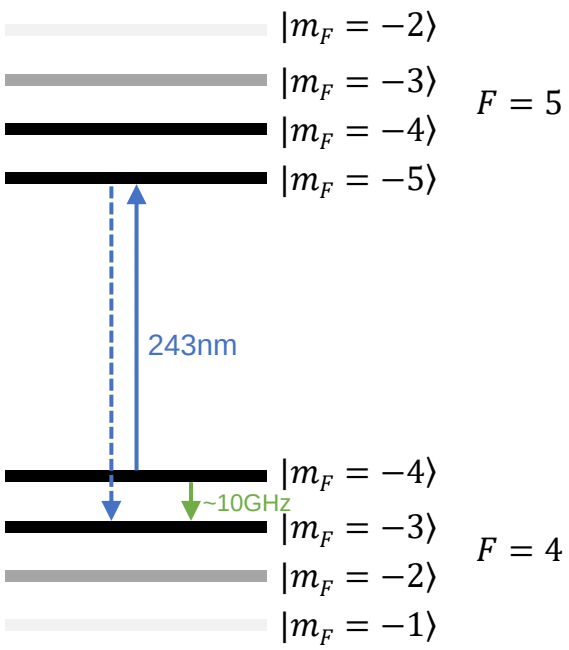

Figure 6.1: Proposed spectroscopy of $^{209}Bi^{82+}$ at ALPHATRAP. The 4 T magnetic field causes a Zeeman splitting for the individual m_F levels. With the techniques discussed in chapter 4, ALPHATRAP allows measuring the 243 nm HFS as well as the 10 GHz Zeeman transitions, which can reveal the nuclear g_I factor.

an astonishing 7σ discrepancy. However, this discrepancy has been traced back to a flawed g_I value, and a careful NMR experiment by LIBELLE made it disappear [72]. At the slightly lower precision resulting from this new g_I value, the QED contributions to $\Delta E'$ are tested to the 20% level. To advance this QED test in strong magnetic fields, first and foremost a clean and precise independent measurement of g_I is needed. ALPHATRAP can provide this, by measuring the Zeeman splitting in the $F = 4$ ground state of the HFS of hydrogenlike (see figure 6.1) or lithiumlike bismuth. The effective g_F-factor can be expressed as

$$g_F = g_J \frac{F(F+1) + J(J+1) - I(I+1)}{2F(F+1)} - g_I \frac{m_e}{m_p} \frac{F(F+1) - J(J+1) + I(I+1)}{2F(F+1)}. \quad (6.2)$$

Consequently, if g_J is known either from theory or from a second measurement of g_F in the $F = 5$ state, g_I can be extracted from g_F, albeit at a $\frac{m_e}{m_p} \approx \frac{1}{1836}$ lower sensitivity. Experimentally, we expect to reach $\delta g_F / g_F < 10^{-10}$, which corresponds to 0.2 ppm precision for g_I. This measurement is possible even if only lithiumlike Bi is available. However, to further improve the QED test, eventually also an improved measurement of the optical HFS transition is required. This is feasible at ALPHATRAP using the techniques discussed in chapter 5.1, but the very small g_F-factor in the $F = 4$ groundstate of ^{209}Bi leads to a correspondingly hard to determine axial frequency jump. While state detection seems possible to achieve with some specialised techniques, our CSGE method does give us more freedom to choose a suitable ion than fluorescence detection does. A specifically interesting candidate in that respect seems to be ^{174}Lu, which has a $F = 1$ groundstate, making the spin detection correspondingly simpler.

In any case, measurements on the hydrogenlike HCI will require the availability of an improved high-energy EBIT. This planned development is topic of the next chapter.

6.2 Enabling measurements in the strongest fields with a new high-energy EBIT for Alphatrap

The main objective of ALPHATRAP, and especially our project within the CRC ISOQUANT, is to perform a stringent test of QED in the $Z\alpha \approx 1$ regime. One prime candidate is hydrogenlike lead $^{208}Pb^{81+}$. This nucleus is doubly magic and has a correspondingly simple structure, which supports the precise prediction of the nuclear contributions to g. Here, $Z\alpha \approx 0.6$ and thus bound-state QED becomes strongly coupled. Consequently, an expansion into orders of $(Z\alpha)^n$ fails and a rigorous calculations in all orders of $Z\alpha$ become necessary. A precise test in this regime would thus enable a new and unique view on strong field physics.

However, the ionisation energy for hydrogenlike $^{208}Pb^{81+}$ is about 105 keV, which is currently out of reach for the Heidelberg HD-EBIT. To efficiently produce $^{208}Pb^{81+}$ an electron beam energy well beyond 200 keV is required. To this end, my group is currently collaborating with the group of PD Dr. José Crespo at MPIK to upgrade the existing Hyper-EBIT to this beam energy. The Hyper-EBIT is much better suited for the high voltages than the HD-EBIT and its cold-head makes it significantly easier and cheaper to operate. Still, many structural and functional parts have to be re-developed and built to satisfy the requirements for isolation distance on the one hand and electromagnetic safety in case of discharges on the other hand. Currently, the Hyper-EBIT is reconstructed in a dedicated laboratory with Faraday cage walls. The plan is to develop the upgrade the Hyper-EBIT in the new offline lab until the required performance can be demonstrated. Then, in a view years, we will relocate it to the current HD-EBIT hut, where it eventually replaces the HD-EBIT. This way, there will be no significant idle time for the experiments at ALPHATRAP as well as for those at the HD-EBIT.

6.3 Sympathetic laser cooling at Alphatrap

Currently, the temperature of the ion motion is a significant limitation for some of our measurements, especially for the laser spectroscopy. While electronic feedback cooling enables $T_z \approx 1\,\mathrm{K}$, mK temperatures are required to reach the Lamb-Dicke regime, where the first-order Doppler effect can be neutralised. Such temperatures are only accessible by laser cooling. However, in many cases the ion of interest does not have suitable cooling transitions. Then, a second ion, e.g. Be^+, is either co-trapped in the same potential, or

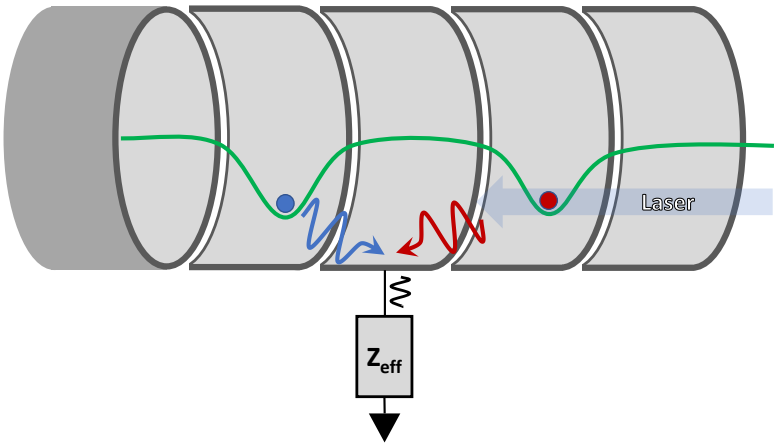

Figure 6.2: Sympathetic laser cooling in separate traps via the image current. The "red" laser-cooled ion is coupled to the "blue" ion of interest via the voltage generated on the shared electrode(s) by their respective image currents. The effective impedance Z decides on the signal amplitude and thus on the coupling rate. If Z is a high-Q tank circuit, the coupling between the ions can be drastically accelerated.

both ions sit in their own potential minima and are coupled via their image currents. The second method has the important advantage that the ion of interest is not exposed to strong Coulomb interactions that would cause motional frequency shifts and hinder a precise determination of the cyclotron frequency. However, this advantage comes at the price of a drastically reduced transfer ("Rabi") frequency Ω_{ex} between ions 1 and 2, which is proportional to the effective impedance $|Z_{\mathrm{eff}}|$ of the image current pickup electrode and the effective electrode distances D_1 and D_2:

$$\Omega_{\mathrm{ex}} = 2\frac{\pi}{\tau_{\mathrm{ex}}} = \frac{1}{2}\frac{q_1 q_2}{\sqrt{m_1 m_2}}\frac{\sqrt{N_1 N_2}}{D_1 D_2}\,|Z_{\mathrm{eff}}|\,. \tag{6.3}$$

Ω_{ex} can be significantly increased by connecting a superconducting tank circuit to the shared electrode(s)[1]. Recently, the BASE collaboration has published first results on sympathetic cooling of protons in separate traps [73, 74]. By tuning both ions into resonance with each other, but slightly off the tank circuit resonance, the relatively large tank impedance increases the coupling rate, while the noise heating from the 4 K tank is limited. In

- Tank circuit assisted sympathetic laser cooling

  B. Tu et al. "Tank-Circuit Assisted Coupling Method for Sympathetic Laser Cooling". In: *Adv. Quantum Technol.* (2021), p. 2100029,

my group has developed a method that supports sympathetic laser cooling of arbitrary ions to mK temperatures. Figure 6.3 shows the predicted effective cooling rate and equilibrium temperature in the "worst case" of a single H_2^+ ion. The effective cooling time constant τ_{eff} is below 10 s even for the largest detunings, which give access to the single mK regime.

[1] This method also works for spatially completely separated traps. In that case, one electrode of each trap is connected to the tank.

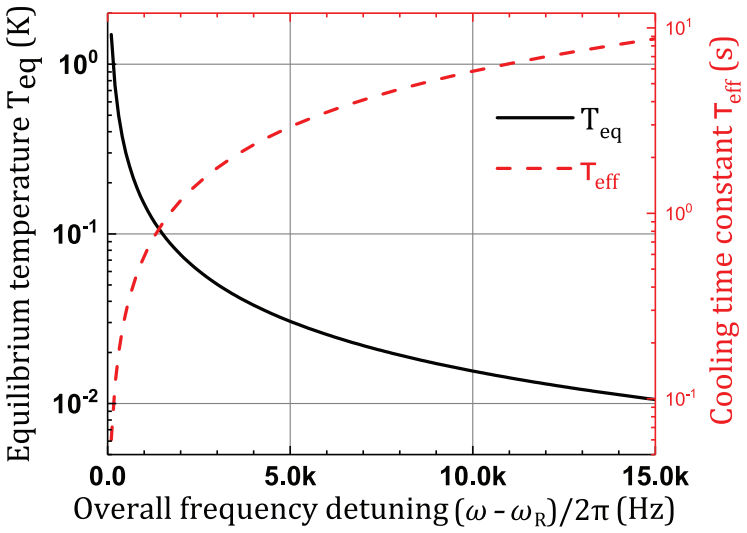

Figure 6.3: Effective cooling rate and equilibrium temperature as a function of the detuning from the tank circuit. In this example, the parameters of the current ALPHATRAP PT tank circuit have been applied for the cooling of a single H_2^+ molecular ion. For HCI the cooling rates would be significantly higher or alternatively the equilibrium temperature could be chosen lower by using a larger detuning. Figure taken from [75].

In combination with a novel trap design, we hope to add sympathetic laser cooling of HCI to our routine toolbox in the near future and thus pave the way for orders-of-magnitude higher precision measurements.

6.4 Fundamental constants and mass differences via the coupled magnetron orbit method

The coupled magnetron orbit method, both for CFR (chapter 3.4.1) and also g-factor differences (chapter 4.3.1), has opened up a new regime of precision for mass- and Zeeman spectroscopy in Penning traps. Specifically the Δg method is extremely versatile, as it profits from the similarity of the Larmor frequencies in many bound-electron systems and has much less strict requirements for the matching of the ion masses than the CFR version.

6.4.1 The finestructure constant α

One obvious application is the determination of fundamental constants, such as the finestructure constant α from a measurement of Δg in low or medium-Z ions. As elaborated in [64], by looking at Δg of two HCI with approximately a factor of two difference in Z, the QED contributions in order $(Z\alpha)^0$ (free electron QED) drop out completely, whereas large parts of the relativistic Dirac contribution, as well as higher order QED contributions remain. A value of α determined from such a Δg would therefore be largely independent of the determination of α from g-2 of the free electron and would consequently support an important consistency checks of the standard model [6, 7, 4].

However, a severe limitation comes from the finite knowledge of the charge radii and other nuclear contributions. These have to be zeroed with the help of additional

measurements, either spectroscopy of muonic atoms (e.g. [76]), XUV and x-ray spectroscopy of electronic HCI [77], or g-factor measurements in other charge states of the same ion [78]. In the latter case, first a specific combination of a lithium- and a hydrogenlike g-factor cancels the nuclear contributions (see chapter 4.3). In a second step, we combine two such specific combinations for different Z ions:

$$\begin{aligned}\Delta_\Omega g &= \Delta_\Xi g(Z) - \Delta_\Xi g(Z/2) \\ &= (g_{2s,Z} - \Xi_Z\, g_{1s,Z}) - \left(g_{2s,Z/2} - \Xi_{Z/2}\, g_{1s,Z/2}\right) \\ &= \left(g_{2s,Z} - g_{2s,Z/2}\right) + \Xi_Z \left(g_{1s,Z} - g_{1s,Z/2}\right) + \left(\Xi_Z - \Xi_{Z/2}\right) g_{1s,Z/2}.\end{aligned} \tag{6.4}$$

It is evident that the dominant contribution comes from the 2s g-factors. In this combination they appear only as differences, which makes them accessible with the extremely precise coupled magnetron orbit method. A similar contribution of 1s g-factors is even reduced by Ξ and the absolute g_{1s} by $\Xi_Z - \Xi_{Z/2} \ll 1$. In [64] the authors show that a precise measurement of $\Delta_\Omega g$ in principle holds promise to improve the precision of α by about an order of magnitude once theory has been sufficiently advanced.

6.4.2 The Q-value of the ^{3}T-^{3}He decay

The KATRIN experiment aims to determine the mass of the electron anti-neutrino or give an upper limit of $m_{\bar{\nu}} < 0.2\,\mathrm{eV}$ by measuring the electron energy spectrum of the ^{3}T beta decay. $m_{\bar{\nu}}$ can be determined from the shape of the spectrum close to the endpoint. If $m_{\bar{\nu}} > 0$, the spectrum is depleted for the highest energies. If the endpoint is known independently from a measurement of the mass difference $\Delta m_{\mathrm{T/He}}$ of ^{3}T-^{3}He, $m_{\bar{\nu}}$ can be constrained better. The $m_{\bar{\nu}} < 0.2\,\mathrm{eV}$ limit that KATRIN aims for translates into a requirement of about $\delta\Delta m_{\mathrm{T/He}}/m_T < 8\,\mathrm{ppt}$. This precision is very difficult to achieve with a traditional alternating CFR measurement, but easily in reach with the common magnetron orbit method. For ^{3}T and ^{3}He the Q-value, or equivalently the mass mismatch, is extraordinarily small. This is desirable to achieve optimal sensitivity to a small anti-neutrino mass, but it also has some implications on the mass difference measurement. Specifically in case of a common magnetron orbit measurement, systematic shifts are very similar for both ions and thus cancel to a large extent. However, the mass difference is actually so small and the trap frequencies are consequently so similar that for realistic separation distances the resonance interaction, or "frequency pulling", becomes excessively large and hinders a precise readout of the CFR. As a workaround it is reasonable to measure ^{3}T and ^{3}He, one at a time, against an auxiliary ion, for example HD^+. There, the mass difference is a bit larger, still small enough to cancel systematics, but large enough to prevent resonant interaction between the ions.

Currently, we are developing the sources that will allow the production of $^3T^+$ and

$^3He^+$ ions in LIONTRAP.

6.5 H_2^+ spectroscopy

The hydrogen molecular ion has been a target for fundamental research for decades. Its uniquely simple structure, with only one electron, makes it very accessible for precision tests. Unlike in atomic systems and especially HCI, molecular hydrogen ions in their electronic ground state have a rich ro-vibrational structure with many levels that can be used for laser spectroscopy. Due to the exact symmetry along the molecular axis, for H_2^+ the dipole moment vanishes and consequently the lifetimes of the ro-vibrational levels (vibrational and rotational quantum numbers (ν, L), respectively) are extremely long [79], ranging up to 2×10^6 s for ro-vibrational transitions and even 1×10^{10} s for the pure rotational transitions (for example $(0, 2) \to (0, 0)$) to the ground state. For the purpose of laboratory experiments we thus have to consider these states to be "stable". On the one hand, this leads to extremely narrow transitions and accordingly high precision, on the other hand the state- and transition detection can be very difficult, respectively impossible with fluorescence detection. Moreover, depending on the production method, many states can be initially populated.

Here, the methods described in chapter 5, based on the CSGE, can be ideally employed. To this end, we make use of the (ν, L) dependence of the $|\downarrow\rangle \leftrightarrow |\uparrow\rangle$ spin transition [80]. By finding the frequency that is able to flip the spin, witnessed by the axial frequency jump due to the CSGE, we can unambiguously determine the (ν, L) state (for $N \geq 2$, even). For sufficiently cold ions (see section 6.3), such measurements can reach 1×10^{-16} relative precision. As the transition frequencies depend on a multitude of fundamental constants, for example the electron-to-proton mass ratio, a comparison to theory prediction allows determining the value of these constants, or alternatively, if we use tabulated values, the

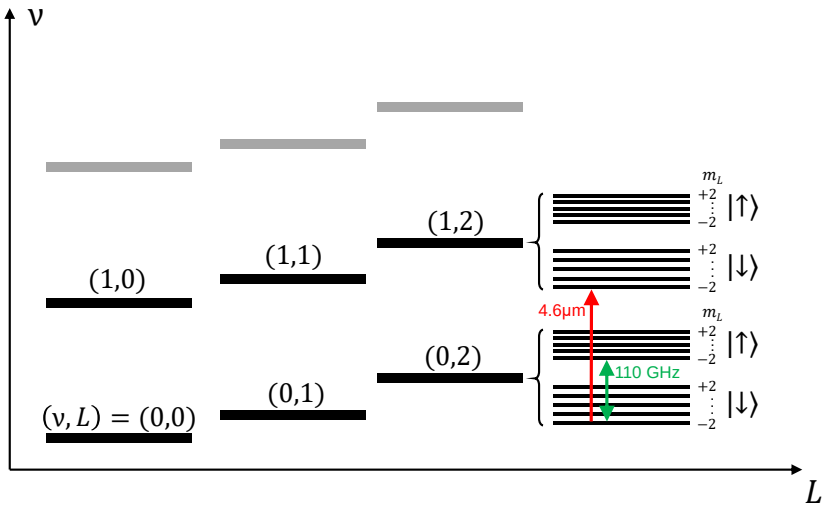

Figure 6.4: Spectroscopy and state detection for H_2^+ or $\bar{H}_2^-$. In this example, a 4.6 μm laser probes the narrow $(0, 2) \to (1, 2)$ transition. As the Larmor frequency is specific for every ν, we can unambiguously determine the (ν, L) state by trying to drive the $|\downarrow\rangle \to |\uparrow\rangle$ with the respective mmW excitation frequencies.

theory prediction can be tested.

As our measurement method requires only a single ion, a very intriguing possibility arises. If it is possible to produce and capture the antimatter equivalent of H_2^+, $\bar{H}_2^-$, the exact same method can be used to measure the respective transitions. A comparison between the transitions in the matter and antimatter ions then constitute a unique and stringent test of the CPT invariance theorem. As CPT demands that the frequencies are exactly identical, no explicit theory prediction of the transition frequencies is required and only the experimental precision is the limit for the comparison. While the conditions in the trap, including the extremely good vacuum, already support this type of measurement, a practical production process for $\bar{H}_2^-$ still needs to be developed. While the constituents, antiprotons and positrons, can be routinely produced and trapped at the antiproton decelerator (AD) facility at CERN, Geneva, the formation of the molecular ion is complicated and inefficient. Still, we hope that in the not too distant future we can implement this fascinating experiment.

7 | Conclusions

Over the last two decades, precision spectroscopy in Penning traps has seen intriguing advances. These have been enabled by the availability of the basic techniques that allow the preparation, cooling and detection of single ions, which have been pioneered in the groups of Hans Dehmelt and later Gerald Gabrielse in Washington and Harvard, David Pritchard at MIT and Günter Werth in Mainz.

At LIONTRAP we have used these techniques, complemented by new developments such as the phase sensitive PnA method and advanced electronics and traps, to determine atomic masses of light ions such as the proton and the deuteron and the HD^+ molecular ion with world-leading precision. These results have shed light on the light ion mass puzzle and revealed inconsistencies in the literature values of these fundamentally important values. In the close future, we plan to also measure the atomic masses of ^{3}He and ^{4}He, which hopefully will resolve this issue.

The availability of highly charged ions in these experiments has added novel opportunities for testing the validity of our standard model in extreme fields. My group has developed and commissioned ALPHATRAP and its predecessor experiment in Mainz[1], which have enabled us to perform a number of unique measurements of the g-factor of the bound electron in single- and few-electron systems:

- $^{28}Si^{13+}$: the most stringent test of QED in strong fields
- $^{28}Si^{11+}$: the most stringent test of relativistic electron interactions in strong fields
- $^{12}C^{5+}$: ultra-precise determination of the electron atomic mass
- $^{40,48}Ca^{17+}$: The isotopic shift of the g-factor beyond the Furry picture

[1] As mentioned earlier, the original version of the Mainz experiment had already been developed in the group of Günter Werth.

- $^{40}Ar^{13+}$:

  g-factor: test of QED in a boronlike, five electron system

  fine-structure: laser spectroscopy of a forbidden transition in HCI

- $^{118}Sn^{49+,47+,45+}$: test of QED in the $Z\alpha \approx 0.36$ regime, currently unpublished

- $^{22,20}Ne^{9+}$: ultra-precise measurement of the isotopic shift with the common magnetron orbit method, test of the QED contribution to the recoil, and limit on physics beyond the standard model, currently unpublished.

The most recent developments of techniques for ultra-precise laser spectroscopy in HCI (chapter 5), ultra-precision spectroscopy of *g*-factor differences with the common magnetron orbit method (chapters 4.3.1 and 3.4.1), and sympathetic laser cooling of arbitrary ions will enable a whole class of intriguing measurements.

Bibliography

[1] S. Sturm et al. "The ALPHATRAP experiment". In: *Eur. Phys. J. Spec. Top.* 227.13 (2019), pp. 1425–1491.

[2] H. Dehmelt. "A single atomic particle forever floating at rest in free space: New value for electron radius". In: *Phys. Script.* 1988.T22 (1988), p. 102.

[3] R. S. Van Dyck Jr, P. B. Schwinberg, and H. G. Dehmelt. "New high-precision comparison of electron and positron g factors". In: *Phys. Rev. Lett.* 59.1 (1987), p. 26.

[4] D. Hanneke, S. Fogwell, and G. Gabrielse. "New measurement of the electron magnetic moment and the fine structure constant". In: *Phys. Rev. Lett.* 100.12 (2008), p. 120801.

[5] H. Dehmelt. "Continuous Stern-Gerlach effect: principle and idealized apparatus". In: *Proc. Natl. Acad. Sci. USA* 83.8 (1986), pp. 2291–2294.

[6] R. H. Parker et al. "Measurement of the fine-structure constant as a test of the Standard Model". In: *Science* 360.6385 (2018), pp. 191–195.

[7] L. Morel et al. "Determination of the fine-structure constant with an accuracy of 81 parts per trillion". In: *Nature* 588.7836 (2020), pp. 61–65.

[8] B. Odom et al. "New measurement of the electron magnetic moment using a one-electron quantum cyclotron". In: *Phys. Rev. Lett.* 97.3 (2006), p. 030801.

[9] V. Debierre, C. Keitel, and Z. Harman. "Fifth-force search with the bound-electron g factor". In: *Phys. Lett. B* 807 (2020), p. 135527.

[10] G. Gabrielse et al. "Towards an improved test of the standard model's most precise prediction". In: *Atoms* 7.2 (2019), p. 45.

[11] G. F. Giudice, P. Paradisi, and M. Passera. "Testing new physics with the electron g-2". In: *J. High Energy Phys.* 2012.11 (2012), p. 113. ISSN: 1029-8479.

[12] B. Abi et al. "Measurement of the positive muon anomalous magnetic moment to 0.46 ppm". In: *Phys. Rev. Lett.* 126.14 (2021), p. 141801.

[13] G. W. Bennett et al. "Final report of the E821 muon anomalous magnetic moment measurement at BNL". In: *Phys. Rev. D* 73.7 (2006), p. 072003.

[14] S. Ulmer et al. “High-precision comparison of the antiproton-to-proton charge-to-mass ratio”. In: *Nature* 524.7564 (2015), pp. 196–199.

[15] S. M. Brewer et al. “$^{27}Al^{+}$ quantum-logic clock with a systematic uncertainty below 10^{-18}”. In: *Phys. Rev. Lett.* 123.3 (2019), p. 033201.

[16] F. Herfurth et al. “The HITRAP facility for slow highly charged ions”. In: *Phys. Scr.* 2015.T166 (2015), p. 014065.

[17] A. Egl et al. “Application of the Continuous Stern-Gerlach Effect for Laser Spectroscopy of the $^{40}Ar^{13+}$ Fine Structure in a Penning Trap”. In: *Phys. Rev. Lett.* 123.12 (2019), p. 123001.

[18] I. Arapoglou et al. “g Factor of Boronlike Argon $^{40}Ar^{13+}$”. In: *Phys. Rev. Lett.* 122.25 (2019), p. 253001.

[19] C. G. Parthey et al. “Improved measurement of the hydrogen 1s–2s transition frequency”. In: *Phys. Rev. Lett.* 107.20 (2011), p. 203001.

[20] S. Alighanbari et al. “Precise test of quantum electrodynamics and determination of fundamental constants with HD^{+} ions”. In: *Nature* 581.7807 (2020), pp. 152–158.

[21] S. Patra et al. “Proton-electron mass ratio from laser spectroscopy of HD^{+} at the part-per-trillion level”. In: *Science* 369.6508 (2020), pp. 1238–1241.

[22] F. Heiße et al. “High-precision mass spectrometer for light ions”. In: *Phys. Rev. A* 100 (2 2019), p. 022518.

[23] G. Gabrielse. “The true cyclotron frequency for particles and ions in a Penning trap”. In: *Int. J. Mass Spectrom.* 279.2-3 (2009), pp. 107–112.

[24] F. Köhler. “Bound-electron g-factor measurements for the determination of the electron mass and isotope shifts in highly charged ions”. PhD thesis. Ruprecht-Karls-Universität Heidelberg, 2015.

[25] J. Ketter et al. “First-order perturbative calculation of the frequency-shifts caused by static cylindrically-symmetric electric and magnetic imperfections of a Penning trap”. In: *Int. J. Mass Spectrom.* 358 (2014), pp. 1–16.

[26] C. Böhm et al. “An ultra-stable voltage source for precision Penning-trap experiments”. In: *Nucl. Instrum. Methods. Phys. Res. A* 828 (2016), pp. 125–131.

[27] S. Rau. “High-precision measurement of the deuteron’s atomic mass”. PhD thesis. Ruprecht-Karls-Universität Heidelberg, 2020.

[28] M. Schuh et al. “Image charge shift in high-precision Penning traps”. In: *Phys. Rev. A* 100.2 (2019), p. 023411.

[29] E. A. Cornell et al. “Mode coupling in a Penning trap: π pulses and a classical avoided crossing”. In: *Phys. Rev. A* 41.1 (1990), p. 312.

[30] B. d'Urso, B. Odom, and G. Gabrielse. "Feedback cooling of a one-electron oscillator". In: *Phys. Rev. Lett.* 90.4 (2003), p. 043001.

[31] S. Rainville, J. K. Thompson, and D. E. Pritchard. "An ion balance for ultra-high-precision atomic mass measurements". In: *Science* 303.5656 (2004), pp. 334–338.

[32] S. Sturm et al. "Phase-sensitive cyclotron frequency measurements at ultralow energies". In: *Phys. Rev. Lett.* 107.14 (2011), p. 143003.

[33] S. Sturm et al. "g-factor measurement of hydrogenlike $^{28}Si^{13+}$ as a challenge to QED calculations". In: *Phys. Rev. A* 87.3 (2013), p. 030501.

[34] Y.-X. Yao and S. M. Pandit. "Cramér-Rao lower bounds for a damped sinusoidal process". In: *IEEE Trans. Signal Process.* 43.4 (1995), pp. 878–885.

[35] P. Singh and A. Singhal. "Frequency estimation of a sinusoidal signal". In: *2016 IEEE Int. Conf. Signal Image Process. ICSIP 2016*. 2016, pp. 320–322. DOI: 10.1109/ICSPCom.2016.7980599.

[36] I. Arapoglou. "First measurement of the ground-state g-factor of boronlike argon $^{40}Ar^{13+}$ in ALPHATRAP". PhD thesis. 2019.

[37] S. Sturm et al. "High-precision measurement of the atomic mass of the electron". In: *Nature* 506.7489 (2014), pp. 467–470.

[38] F. Heiße et al. "High-precision measurement of the proton's atomic mass". In: *Phys. Rev. Lett.* 119.3 (2017), p. 033001.

[39] S. Rau et al. "Penning trap mass measurements of the deuteron and the HD^+ molecular ion". In: *Nature* 585.7823 (2020), pp. 43–47.

[40] E. Tiesinga et al. "CODATA recommended values of the fundamental physical constants: 2018". In: *Rev. Mod. Phys.* 93 (2 2021), p. 025010.

[41] M. Wang et al. "The AME 2020 atomic mass evaluation (II). Tables, graphs and references". In: *Chin. Phys. C* 45.3 (2021), p. 030003.

[42] E. G. Myers et al. "Atomic masses of tritium and helium-3". In: *Phys. Rev. Lett.* 114.1 (2015), p. 013003.

[43] R. S. Van Dyck Jr et al. "High precision Penning trap mass spectroscopy and a new measurement of the proton's "atomic mass"". In: *AIP Conf. Proc.* Vol. 457. American Institute of Physics. 1999, pp. 101–110.

[44] S. L. Zafonte and R. S. Van Dyck Jr. "Ultra-precise single-ion atomic mass measurements on deuterium and helium-3". In: *Metrologia* 52.2 (2015), p. 280.

[45] D. J. Fink and E. G. Myers. "Deuteron-to-Proton Mass Ratio from the Cyclotron Frequency Ratio of H_2^+ to D^+ with H_2^+ in a Resolved Vibrational State". In: *Phys. Rev. Lett.* 124.1 (2020), p. 013001.

[46] I. Kortunov et al. “Proton–electron mass ratio by high-resolution optical spectroscopy of ion ensembles in the resolved-carrier regime”. In: *Nat. Phys.* 17.5 (2021), pp. 569–573.

[47] M. Redshaw et al. “Mass ratio of two ions in a Penning trap by alternating between the trap center and a large cyclotron orbit”. In: *Int. J. Mass Spectrom.* 251.2-3 (2006), pp. 125–130.

[48] E. A. Cornell et al. “Two ions in a Penning trap: Implications for precision mass spectroscopy”. In: *Physical Review A* 45.5 (1992), p. 3049.

[49] J. K. Thompson. “Two-ion control and polarization forces for precise mass comparisons”. PhD thesis. Massachusetts Institute of Technology, 2003.

[50] S. Sturm et al. “g factor of hydrogenlike $^{28}Si^{13+}$”. In: *Phys. Rev. Lett.* 107.2 (2011), p. 023002.

[51] A. Wagner et al. “g factor of lithiumlike silicon $^{28}Si^{11+}$”. In: *Phys. Rev. Lett.* 110.3 (2013), p. 033003.

[52] D. Glazov et al. “g Factor of Lithiumlike Silicon: New Challenge to Bound-State QED”. In: *Phys. Rev. Lett.* 123.17 (2019), p. 173001.

[53] F. Köhler et al. “Isotope dependence of the Zeeman effect in lithium-like calcium”. In: *Nat. Commun.* 7.1 (2016), pp. 1–8.

[54] F. Köhler et al. “The electron mass from g-factor measurements on hydrogen-like carbon $^{12}C^{5+}$”. In: *J. Phys. B-At. Mol. Opt.* 48.14 (2015), p. 144032.

[55] J. Bergquist et al. “Observation of quantum jumps in a single atom”. In: *Phys. Rev. Lett.* 57.14 (1986), p. 1699.

[56] S. Faruque. *Radio frequency modulation made easy*. Springer, 2017.

[57] T. Beier et al. “g_j Factor of an electron bound in a hydrogenlike ion”. In: *Phys. Rev. A* 62.3 (2000), p. 032510.

[58] Z. Harman. *Private communication with Dr. Zoltán Harman*.

[59] H. Häffner et al. “High-accuracy measurement of the magnetic moment anomaly of the electron bound in hydrogenlike carbon”. In: *Phys. Rev. Lett.* 85.25 (2000), p. 5308.

[60] J. Verdú et al. “Electronic g Factor of Hydrogenlike Oxygen $^{16}O^{7+}$”. In: *Phys. Rev. Lett* 92.9 (2004), p. 093002.

[61] V. Yerokhin et al. “Self-energy screening effects in the g factor of Li-like ions”. In: *Phys. Rev. A* 102.2 (2020), p. 022815.

[62] M. Hori et al. “Two-photon laser spectroscopy of antiprotonic helium and the antiproton-to-electron mass ratio”. In: *Nature* 475.7357 (2011), pp. 484–488.

[63] D. L. Farnham, R. S. Van Dyck Jr, and P. B. Schwinberg. “Determination of the electron’s atomic mass and the proton/electron mass ratio via Penning trap mass spectroscopy”. In: *Phys. Rev. Lett.* 75.20 (1995), p. 3598.

[64] V. Yerokhin et al. “g Factor of Light Ions for an Improved Determination of the Fine-Structure Constant”. In: *Phys. Rev. Lett.* 116.10 (2016), p. 100801.

[65] C. Solaro et al. “Improved Isotope-Shift-Based Bounds on Bosons beyond the Standard Model through Measurements of the D 2 3/2- D 2 5/2 Interval in Ca+”. In: *Phys. Rev. Lett.* 125.12 (2020), p. 123003.

[66] M. Bordag et al. *Advances in the Casimir effect*. Vol. 145. OUP Oxford, 2009.

[67] J. Redondo and G. Raffelt. “Solar constraints on hidden photons re-visited”. In: *J. Cosmol. Astropart. Phys.* 2013.08 (2013), p. 034.

[68] C. Delaunay et al. “Probing new spin-independent interactions through precision spectroscopy in atoms with few electrons”. In: *Phys. Rev. D* 96.11 (2017), p. 115002.

[69] P. O. Schmidt et al. “Spectroscopy using quantum logic”. In: *Science* 309.5735 (2005), pp. 749–752.

[70] B. Bransden and C. Joachain. *Physics of atoms and molecules*. Essex: Longman Scientific & Technical, 1983.

[71] J. Ullmann et al. “High precision hyperfine measurements in Bismuth challenge bound-state strong-field QED”. In: *Nat. Commun.* 8.1 (2017), pp. 1–7.

[72] L. V. Skripnikov et al. “New Nuclear Magnetic Moment of ^{209}Bi: Resolving the Bismuth Hyperfine Puzzle”. In: *Phys. Rev. Lett.* 120.9 (2018), p. 093001.

[73] M. Bohman et al. “Sympathetic cooling of a trapped proton mediated by an LC circuit”. In: *Nature* (2021), pp. 1–5.

[74] M. Bohman et al. “Sympathetic cooling of protons and antiprotons with a common endcap Penning trap”. In: *J. Mod. Opt.* 65.5-6 (2018), pp. 568–576.

[75] B. Tu et al. “Tank-Circuit Assisted Coupling Method for Sympathetic Laser Cooling”. In: *Adv. Quantum Technol.* (2021), p. 2100029.

[76] J. J. Krauth et al. “Measuring the α-particle charge radius with muonic helium-4 ions”. In: *Nature* 589.7843 (2021), pp. 527–531.

[77] H. Cakir et al. “Improved access to the fine-structure constant with the simplest atomic systems”. In: *arXiv preprint arXiv:2006.14261* (2020).

[78] V. Yerokhin et al. “Weighted difference of g factors of light Li-like and H-like ions for an improved determination of the fine-structure constant”. In: *Phys. Rev. A* 94.2 (2016), p. 022502.

[79] A. Posen, A. Dalgarno, and J. Peek. “The quadrupole vibration-rotation transition probabilities of the molecular hydrogen ion”. In: *At. Data Nucl. Data Tables* 28.2 (1983), pp. 265–277.

[80] E. G. Myers. “CPT tests with the antihydrogen molecular ion”. In: *Phys. Rev. A* 98.1 (2018), p. 010101.